Democratic and popular Republic of Algeria

Ministry of Higher Education and Scientific Research

Polytechnic National School

Development center for Renewable energies

DOCTORAL SCHOOL FOR RENEWABLE ENERGIES

MASTER THESIS

Subject: Renewable Energies

Option: Photo thermal

Topic

Determination of Maximum Recoverable Heat in a Thermodynamic combined cycle (solar-gas) with a steam turbine downstream the power plant.

Submitted by: Omar BEHAR

To the following Jury members:

Mr. Cherif LARBES	Professor (ENP)	Jury president
Mr. Salah LARBI	Professor (ENP)	Examiner
Mr. Abdallah KHELAF	R.D (CDER)	Examiner
Mm. Nachida MERZOUK	R.D (CDER)	Examiner
Mr. Maiouf BELHAMEL	R.D (CDER)	Supervisor
Mr. Mourad HADDADI	Professor (ENP)	Invited

Academic year: 2009 – 2010

BISMILLAHIRRAHMANIRRAHIM

IN THE NAME OF ALLAH THE MOST MERCIFUL

- *Thank you GOOD so much for your Help and guidance.*

ACKNOWLEGMENTS

I would like to thank Dr. Maiouf BELHAMEL, my supervisor, for His kindness and help. His worthy advice and his valuable academic assistance are acknowledged.

I express my sincere appreciation to Mr. Ahmed HADIOUCHE for his guidance throughout this research.

I am especially grateful for the feedback and support of all of the polytechnic national school (ENP) and the development center of renewable energies (CDER) staff.

Best thanks to my family for their understanding, motivation and patience.

Finally, a special thank you goes to all of my friends in the doctoral school for renewable energies.

ملخص

الهدف من هذا البحث هو تطوير برنامج لأول محطة كهربائية هجينة (طاقة شمسية- غاز طبيعي) في الجزائر وذالك تحت مناخ منطقة حاسي الرمل. في هذا المشروع نقترح محطة بدرجة واحدة من الضغط. عند وجود الشمس يتم تحسين تحويل طاقة الانبعاث الغازية المطروحة من العفنة الغازية في العفنة البخارية باستعمال مبادل شمسي $HSSG$ بالتوازي مع مبادل غازي $HRSG$. هذا التصميم يعطي ليونة في التشغيل, حيث يمكن للمحطة أن تعمل كلاسيكيا CC في الليل و أن تعمل كمحطة هجينة في النهار. المردود الحراري و كمية الكهرباء المنتجة هم أهم العوامل لتحديد أداء المحطة عبر أيام السنة. نتائج البرنامج بينت أن هده المحطة بإمكانها توليد ما يقارب 134 ميقا واط بمردود يساوي 57.5% خلال الليل. في النهار نسبة الكهرباء الناتجة عن الطاقة الشمسية جد محفزة حيث يمكن أن تصل إلى 15% في الفترات الجد مشمسة. عندها تكون كمية الكهرباء المنتجة و مردود المحطة اكبر ب 17 و 16.5% على التوالي من عملها كمحطة كلاسيكية, ما يقابله 157 ميقا واط من الطاقة بمردود 67%. زيادة قدرة العفنة البخارية ب 50% و أحسن أداء للمحطة الهجينة في صحراء حاسي الرمل خلال الأيام الحارة هي محاسن أخرى للتصميم المقترح.

مفاتيح: محطة كهربائية هجينة (طاقة شمسية- غاز طبيعي), محطة كهربائية شمسية, حاسي الرمل.

RESUME

Le but de cette étude est de développer un programme de calcul pour l'analyse des performances énergétiques de la première centrale hybride solaire-gaz (ISCCS) en Algérie, sise à Hassi R'mel. Dans ce projet une centrale avec un niveau de pression est proposée. Durant les périodes ensoleillées, la conversion de l'énergie des gaz d'échappements dans la turbine à vapeur est améliorée par l'utilisation d'un échangeur solaire (HSSG) en parallèle avec la chaudière à vapeur (HRSG). Ce concept donne une certaine flexibilité pour son fonctionnement, il fonctionne en mode combiné conventionnel durant la nuit et en mode hybride solaire-gaz durant la journée. Le rendement thermique et l'énergie électrique produite sont les principaux paramètres pour évaluer les performances instantanées des différentes parties de la centrale durant l'année. Les résultats de ce program montrent que cette centrale peut fournir environ 134MW de puissance avec un rendement de 57,5% dans la nuit. Dans la journée, le ratio net du solaire peut être très intéressant et atteindre les 15%. En conséquence, l'électricité produite par la centrale et son rendement seront plus importants de 17 et 16,5% respectivement qu'en mode combine, ce qui correspond à une puissance de 157MW et un rendement de 67%. L'augmentation de la capacité de la turbine à vapeur de 50% et les meilleurs performances de la centrale hybride pour les journées chaudes à Hassi R'mel sont les avantages supplémentaires de ce concept.

Mots clés : centrale thermodynamique solaire avancées, centrale thermique solaire, Hassi R'Mel.

ABSTRACT

The purpose of this study is to develop a mathematical program for analysing the performance of the first integrated solar combined cycle system (ISCCS) in Algeria, located in Hassi R'mel. In this project, an integrated plant with simple pressure level is proposed. During sunny periods, the energy conversion of the exhaust gas in the steam turbine is improved by using solar heat steam generator HSSG in parallel with the heat recovery steam generator HRSG. This design furnishes flexibility in the operation system where it works as a conventional combined cycle during night time and it switches to operate as an ISCCS during daylight. Thermal efficiency and electricity generating are the main parameters to evaluate the instantaneous performances of different parts of the solar power plant through the year. The program results show that the power plant would produce about 134MW with efficiency equal to 57.5% at night. At daytime, the net solar electricity ratio can be very interesting and reach the limit of 15% at the design point. As a result, the output from and the efficiency of the integrated plant will be above the CC regime by 17 and 16.5%, which correspond to 157MW and 67%, respectively. Increasing the steam turbine capacity by 50% and better performances of the integrated plant in Hassi R'mel desert in warm days are other advantages of the proposed design.

Key Words: Integrated solar combined cycle system, solar thermal power plant, Hassi R'Mel.

ABBREVIATIONS

CC	Combined Cycle
CD	Condenser
Cc	Combustion Chamber
DSG	Direct Steam Generation
EC	Economizer
ET	Euro Trough Collector
EU-MENA	Europe, Mediterranean North African region
EX	Heat Exchanger
FP	Feed Water Pump
GT	Gas Turbine Unit
HCE	Heat Collection Element
HRSG	Heat Recovery Steam Generator
HSSG	Heat Solar Steam Generator
HTF	Heat Transfer Fluid
HVDC	High Voltage Direct Current
ISCCS	Integrated Solar Combined Cycle System
K	Axial compressor
LEC	Levelized Energy Cost
LS	Luz System
PTC	Parabolic Trough Collector
SEGS	Solar Electricity Generating System
SF	Solar Filed
SG	Steam Generator
SH	Superheater
SGT	Siemens Gas Turbine
SST	Siemens Steam Turbine
ST	Steam Turbine unit
TRANS-CSP	Trans-Mediterranean Interconnection for Concentrating Solar Power
TREC	Trans-Mediterranean Renewable Energy Cooperation

NOMENCLATURE

Symbols	Parameters	Units
A_{abs}	Outer area of the absorber	[m^2]
A_{ap}	Collector aperture area	[m^2]
A_{loss}	loss area	[m^2]
a_p	Aperture of the concentrator	[m]
A_{SF}	Solar field area	[m^2]
C_c	Geometric concentration ratio	---
C_L	Number of collectors in each row	---
Cp_g	Average specific heat of the exhaust gases in the HRSG	[J/kg. K]
Cp_V	Average specific heat of the steam in the HRSG	[J/kg. K]
d	Receiver diameter	[m]
DNI	Direct normal irradiation	[W/m^2]
dP	Pressure losses	[Pa]
E	The equation of time	[min]
f	Focus length of the concentrator	[m]
I_d	Diffuse radiation	[W/m^2]
I_{sc}	Solar constant	[W/m^2]
I_{so}	Extraterrestrial radiation	[W/m^2]
I_T	Terrestrial solar radiation	[W/m^2]
$K(\theta)$	Incidence angle modifier	---
L_d	Number of daylight hours	[h]
L_{loc}	Longitude of the location	[Degree]
L_{st}	Standard meridian for the local time zone	[Degree]
n_j	Number of the day	---
N_L	Number of line in the solar field	---
m_R	Cooling air mass flow rate	[%]
m_k	Compressor air mass flow rate	[kg/s]
M_f	Gas turbine fuel consumption	[kg/h]
m_{sf}	HTF mass flow rate	[kg/s]
m_R	Relative air mass flow rate for blades cooling	[%]
m_f	Fuel mass flow rate	[%]
m_g	Mass flow of exhaust gases	[kg/s]
m_{so}	HSSG seam mass flow	[kg/s]
m_s	Steam mass flow of heat exchangers	[kg/s]

P_a	Atmospheric pressure	[Pa]
P_{se}	Inlet steam pressure of heat exchangers	[Pa]
P_{ss}	Outlet steam pressure of heat exchangers	[Pa]
Q_{cv}	Gas natural calorific value	[MJ/kg]
Q_{gas}	Exhaust gas energy per unit of time	[MW]
Q_c	Useful energy gained by the collector per unit of time	[MW]
Q_{SF}	Total useful energy gained in the SF per unit of time	[MW]
Q_R	The extraction heat in the cooling air per unit of time	[MW]
R	The gases constant	[J/kg.K]
R_{so}	The solar electricity ratio	[%]
sfc	Specific fuel consumption	[MJ/kW.h]
Si	Standard time	[h]
Sr	Sunrise time	[h]
Ss	Sunset time	[h]
T_a	Ambient temperature	[°C]
T_b	Turbine blade temperature	[°C]
T_R	Cooling air outlet temperature	[°C]
T_{abs}	Mean absorber pipe temperature	[°C]
$T_{ge\,1}$	Inlet temperature of exhaust gases at heat exchangers	[°C]
T_{gs}	Outlet temperature of exhaust gases at heat exchangers	[°C]
T_{se}	Inlet steam temperature of heat exchangers	[°C]
T_{ss}	Outlet steam temperature of heat exchangers	[°C]
T_{so}	Steam outlet temperature of HSSG	[°C]
W_{GT}	Total specific work of GT	[kJ/kg]
W_{GT}^{net}	Gas turbine output	[MW]
W_{FP}	Feed water pump specific work	[kJ/kg]
W_k	Compressor specific work	[kJ/kg]
W_T	Gas turbine specific work	[kJ/kg]
W_{SR}	Relative work for gases without the air cooling system	[kJ/kg]
W_{ST}	Steam turbine specific work	[kJ/kg]
W_{ST}^{net}	Steam turbine output	[MW]

GREEK SYMBOLS

Symbols	Parameters	Units
η_{opt}	Optical efficiency	--
η_s^k	Compressor isentropic efficiency	--
η_p^k	Compressor polytropic efficiency	--
γ_k	Specific heat ratio	--
η_{cc}	Combustion chamber efficiency	--
η_{is}^T	Turbine isentropic efficiency	--
η_p^T	Turbine polytropic efficiency	--
η_{GT}	Gas turbine unit efficiency	--
η_{ST}	Steam turbine efficiency	--
η_{ISCCS}	ISCCS efficiency	--
$\propto_o$	The air to fuel ratio for combustion	--
$\propto_a$	Excess air coefficient	--
$\propto_g$	Excess air coefficient of exhaust gas	--
ά	The dispersion angle	[Degree]
ε_R	Cooling system effectiveness	--
ξ_R	Expansion coefficient of cooling air	--
σ_T	Ganses expansion ratio	--
δ	Declination angle	[Degree]
θ_z	Zenith angle	[Degree]
θ	Angle of incidence	[Degree]
θ_α	Half Acceptance angle	[Degree]
α_s	Solar altitude angle	[Degree]
β	Slop of the surface	[Degree]
γ	Surface azimuth angle	[Degree]
γ_s	Solar azimuth angle	[Degree]
ω	Hour angle	[Degree]
ω_s	Sunset hour angle	[Degree]
ε	Earth's Eccentricity	[Degree]
φ_R	Rim angle	[Degree]
Φ	Latitude	[m]

LIST OF FIGURE

LIST OF TABLE

TABLE OF CONTENTS

INTRODUCTION

Algeria is situated in North Africa and has large areas that receive solar energy. It has a considerable potential for solar power plants. About 84% of Algeria is consisted of deserts which receive incredible amount of solar irradiation. If a little part of these areas can be covered by solar collectors, energy obtained will be more than annual electricity production in Algeria.

Hybrid solar thermal power plants with parabolic trough solar collectors, featuring gas burners and Rankine steam cycles have been successfully demonstrated by California's Solar Electric Generating System (SEGS). This system has been proven to be one of the most efficient and economical schemes to convert solar energy into electricity. Although these plants are clearly optimized for their particular conditions, other power cycle designs may be appropriate in other situations. Of particular interest is the integration of parabolic trough solar technology with combined cycle power plant. This configuration is referred to integrated solar combined cycle systems (ISCCS).

Integrated solar combined cycle systems are modern combined cycle power plants with gas and steam turbines and additional thermal input of solar energy from a field of parabolic troughs. The plant concept was initially proposed by Luz Solar International.

An ISCCS offers three principal advantages. First, solar energy can be converted to electric energy at a higher efficiency. Second, the incremental unit costs for the larger steam turbine in the integrated

plant are less than the overall unit cost in a (SEGS). Third, an integrated plant does not suffer the thermal inefficiencies associated with the daily start up and shutdown of the steam turbine. This advanced power plant can work in three modes: Integrated solar combined cycle mode at solar hours, conventional combined cycle mode at non solar hours and gas turbine mode when the steam turbine is not functioning.

The aim of this study is to develop a mathematical program for analysing the performance of the first integrated solar combined cycle system in Algeria under Hassi R'mel climatic conditions. In this work, an integrated plant with simple pressure level is proposed. During sunny periods, the energy conversion of the exhaust gas in the steam turbine is improved by using solar heat steam generator HSSG in parallel with the heat recovery steam generator HRSG.

Solar energy fundamentals and the details of the selected solar collector are presented in the first chapter. The second and the third chapters deal with the ISCCS (details and thermodynamic analysis). The simulation and results of each part of the integrated power plant are clearly described in the last chapter.

BIBLIOGRAPHY STUDY

Parabolic trough concentrator (PTC) has been used for more than 100 years. Initially, PTC was used for small scale solar thermal mechanical applications, with outputs up to 100 kW, mainly for water pumping (Duffie and Beckman, 1991). Only after the energy crises of 1973 did the idea of large scale solar power plants take hold (Thomas and Guven 1993). Starting in the late 1980s, nine solar electric generating systems (SEGS) have been built and operated in the Mojave Desert of Southern California.

Nowadays, the Integrated Solar Combined Cycle system (ISCCS) offers an effective means for the continued development of parabolic trough technology (Bruce Kelly et al., 2001). This advanced solar thermal power plant was initially proposed by Luz Solar International since the early 1990s, as a mean of integrating a parabolic trough solar field with modern combined cycle power plant. Due to the decision of the Global Environment Facility, in 2000, to provide grants for four ISCCS power plants in India, Egypt, Morocco and Mexico, interest in this kind of power plants increases day after day.

The ISCCS represents both economically and energetically a promising alternative for the conversion of solar energy while offering a guarantee of a minimum power supply independent of the level of solar radiation (Favrat, 1995; Allani and Favrat, 1991). Its performances are, however, strongly dependent on the intensity of the solar input and of the method of transferring solar energy into the combined cycle.

The thermo economical criteria (performances/ costs) of such integrated power plants is considerably more complex than for conventional plants because the integrated plant must take into account the variations in solar energy availability during the year (Buck et al., 1998).

Some optimal designs for several different plant configurations linked to the pilot plant project in Tunisia were determined using a quasi stationary thermo economic approach which uses a hierarchical structure to determine configuration, component design (size and performance) and system operation is proposed by (Allani et al., 1997). The basic idea is to have an oversized steam turbine. As this turbine reaches the fall load when beam radiation is the highest, the gas turbine load is progressively decreasing while the steam turbine is kept at full load. This concept

does not take into account the performance of the gas turbine especially when the solar energy is higher.

For the same project with the aim of optimising the ISCCS, (Kane and Favrat, 1999) concentrated their studies on the heat exchangers network. They used the data of the turbines and the solar field to optimise the choice of the pressure level and the mass flow. In the first part they employed the classical pinch technology principals coupled with a mathematical programming algorithm in order to minimize the heat transfer exergy losses. Relating to the steam turbine conditions implies that the minimum pinch point cannot be kept and the heat exergy losses are higher with solar energy input. To achieve the maximum efficiency of the various operational modes, an analysis introduces a new steam interaction factor is used to define the mass flow and to design the heat exchangers network.

(Kane and Favrat, 2000) tried again for the optimal designs of the heat exchanger network. Thus, a mixed approach based on pinch technology coupled with a mathematical optimisation algorithm to minimise the heat exergy losses in the HRSG was adapted.

In order to reduce components and better exploiting the exergy potential of the working fluid, the direct steam generation (DSG) technology is used to generate solar steam which is supplied to the steam turbine to increase the power output during the sunny periods. For this reason, a mathematical program was developed to simulate the ISCCS performance under Libyan climatic conditions (elsaket, 2007). The inherent complexity of heater integration within standard gas turbines is a major hindrance to the introduction of this concept.

Some optimization studies for ISCCS are also proposed by (Bruce et al. 2001). During the investigation process, several plants design and cycle balance calculations were performed using the commercial computer codes GateCycle and IPESpro. Steady performance for different load cases was calculated. They found that an ISCCS with a single pressure level offers an effective mean for the continued development of this type of power plants and present the lowest cost comparing with other configurations.

In this kind of power plants, the most efficient method for converting solar thermal energy to electric energy is to withdraw feed water from the heat recovery steam generator downstream of economizer, produce high pressure saturated steam using solar energy, and return the steam to

the heat recovery steam generator (HRSG) for superheating by the gas turbine exhaust. (Bruce et al. 2001)

An integrated plant without thermal storage provides an interesting way for solar electricity generating and gives better solutions than SEGS plants. In comparison to the Rankine cycle of this latter, ISCCS plants offer three principal advantages: First, solar energy can be converted to electric energy at a higher efficiency. Second, the incremental costs for a larger steam turbine are less than the overall unit cost in a solar only plant. Third, an integrated plant does not suffer from the thermal inefficiencies associated with the daily start up and shutdown of the steam turbine (Dersch et al., 2004).

The comparison of different power plants with ISCCS show that an integrated solar power plant without auxiliary firing have the lowest LEC, which is about 10 and 33% lower than combined cycle and gas turbine, respectively, If we consider the environmental effects. (Hosseini et al., 2005).

Even though the evaluation of combined cycle power plants can be performed by using the mean values of ambient temperature, load and full load hours, ISCCS are considerably more affected by ambient conditions and load profiles. Therefore, it is essential to use annual performance calculations for ISCCS plant analysis. (Bruce et al. 2001)

The purpose of this research is to develop a mathematical program for the first integrated solar power plant in Algeria. This ISCCS will be built in Hassi R'mel desert. The selected site has an elevation of 776 m. In this project an integrated plant with simple pressure level is proposed. The energy conversion of the exhaust gases in the steam turbine is improved by using solar evaporator HSSG in parallel with the heat recovery steam generator. The mathematical program will be used to simulate instantaneous performances of the ISCCS under Hassi R'mel climatic conditions during the year. The effect of the ambient temperature and solar energy fluctuation on the performance of the integrated plant is also evaluated by this program.

1. SOLAR ENERGY FUNDAMENTALS AND PARABOLIC TROUGH COLLECTOR

1.1. Solar energy fundamentals

The sun is an effective black body whose outer surface has a temperature of 5777 k and emitting an incredible amount of solar radiation into every corner of space appears in the form of electromagnetic waves that carry energy at the speed of light. The solar radiation is absorbed, reflected, or diffused by solid particles in any location of space and especially by the earth, which depends on its arrival for many activities such as climate type. Depending on the geometry of the earth, its distance from the sun, geographical location of any point on the earth, astronomical coordinates, and the composition of the atmosphere, the incoming irradiation at any given point takes different shapes. This section provides the basic concepts, definitions, and derived astronomical equations furnish the foundations of solar energy evaluation at any given location.

1.1.1 Solar radiation as it is travels through the atmosphere

Solar radiation from the sun after travelling in space enters the atmosphere at the space-atmosphere interface, where the ionization layer of the atmosphere ends. Afterwards, a certain amount of solar radiation or photons are absorbed by the atmosphere, clouds, and particles in the atmosphere, a certain amount is reflected back into the space, and a certain amount is absorbed by the earth's surface.

The sun: The sun has played a dominant role since time immemorial for different natural activities in the universe at large and in the earth in particular for the formation of fossil and renewable energy sources. It is a big ball of plasma. The Plasma is a state of matter where the electrons are separated from the nuclei because the temperature is so high and accordingly the kinetic energies of nuclei and electrons are also high. The radiating power of the sun results from a process in which four hydrogen nuclei fuse into a helium nucleus. The resulting loss of mass, totalling 4.3 million tons per second is transferred into a freed power by irradiance to the space.

Solar constant (I_{sc}): the solar constant denoted by I_{sc} is the energy from the sun per unit time received on a unit surface area perpendicular of the direction of propagation of radiation at the earth mean distance from the sun outside the atmosphere.

The World Radiation Center has adapted a value of 1367 Watts per square meter, with an uncertainty of the order of 1% (Duffie and Beckman, 1991).

Extraterrestrial radiation (I_{so}): is the radiation that would be received in the absence of the atmosphere. The change in the extraterrestrial radiation can be caused by two sources:

Variation in radiation emitted by the sun: there are conflicting reports in the literature on periodic variation of intrinsic solar radiation. It has been suggested that there is small variation with different periodicities and variation related to sunspot activities. Hence, data from Nimbus and Mariner satellites over several months were used. For instance, (Hickey et al., 1982) during two years and a half found that the solar constant is decreasing slowly, at the rate of approximately 0.02% per year. In this research the solar constant is considered invariable.

Variation of earth-sun distance: the earth rotates around the sun in an elliptical orbit. This movement results in variation in an earth-sun distance by 1.7%. Therefore, the extraterrestrial radiation varies in a range of ±3%.

The change in I_{so} can be calculated by taking into account the astronomical facts according to the following approximation formula: (Duffie and Beckman, 1991)

$$I_{so} = I_{sc}[1 + 0.033\cos(360\, n_j/365)] \quad (1.1)$$

Where n_j is the number of the day corresponding to a given date. It is defined as the number of days elapsed in a given year up to a particular date starting from 1 on 1 January to 365 on 31 December.

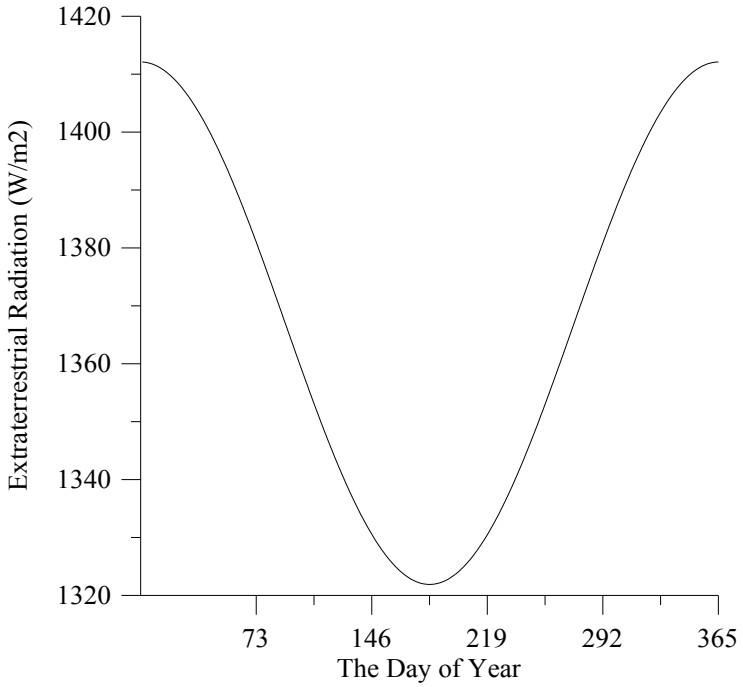

Figure1.1: Variation of extraterrestrial radiation with time of year.

Attenuation of solar radiation by the atmosphere: Solar radiation at normal incidence received at the surface of the earth is subject to vary due to change in the extraterrestrial radiation and to two additional more significant phenomena. These are the atmospheric scattering by air molecules, water vapor and dust and the atmospheric absorption especially by ozone and water. The effects of the atmosphere in absorbing and scattering solar radiation are variable with time as atmospheric conditions and the air mass ratio change. It can be weighed up by the atmospheric transmittance factor.

Atmospheric transmittance values vary with location and elevation between 0 and 1. According to (Gates, 1980) at very high elevations with extremely clear air may be as high as 0.8, while for a clear sky with high turbidity it may be as low as 0.4. As shown in Fig 1.2, the solar radiation during its travel through the atmosphere toward the earth surface meets various phenomena, including scatter, absorption, reflection, diffusion, meteorological conditions, and air mass, which change with time.

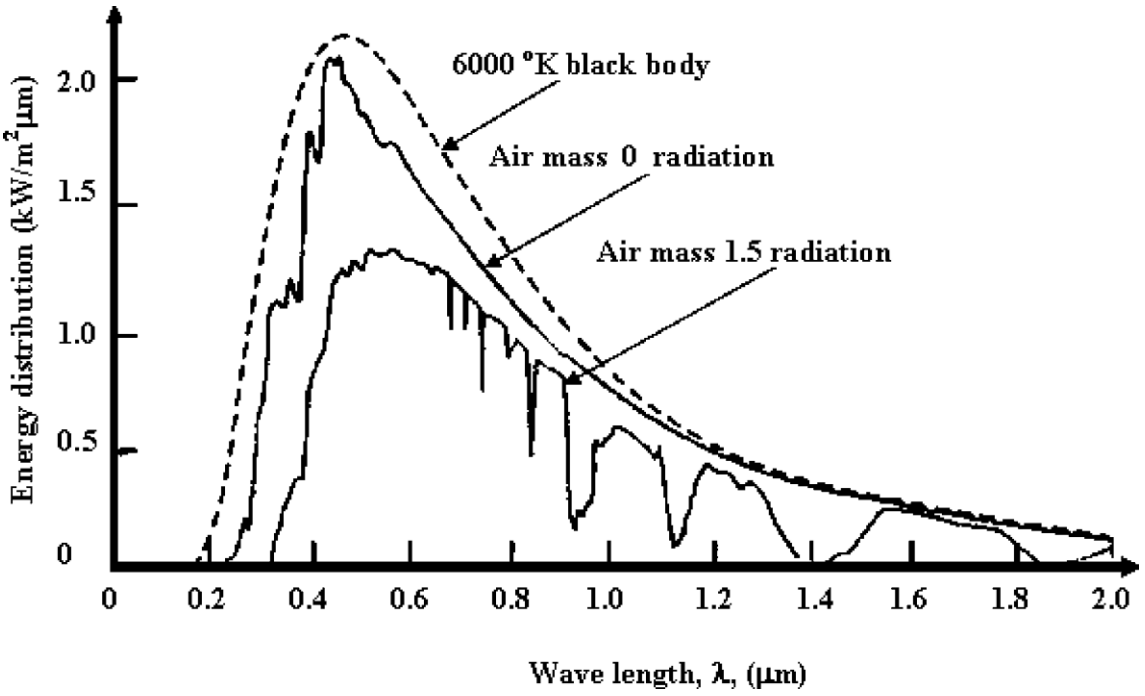

Figure 1.2: Solar spectrums (zekai sen, 2007).

It is useful to define a standard atmosphere clear sky and calculate the hourly and daily radiation that would be received on a horizontal surface under these standard conditions. (Hottel, 1976) has presented a method of estimating the beam radiation transmitted through a clear atmosphere and he introduced four climate types as in Table 1.1. The atmospheric transmittance for beam radiation (τ_b) is given in an exponentially decreasing form depending on the altitude (α_s) and zenith angle (θ_z) as:

$$\tau_b = a + b \exp\left(-\frac{c}{\cos(\theta_z)}\right) \tag{1.2}$$

The estimations of constants a, b, and c for the standard atmosphere with 23 km visibility is given by (Kreith and Kreider, 1978):

$$a = [0.4237 - 0.00821(6 - \alpha_s{}^2)]\, a_o \tag{1.3}$$

$$b = [0.5055 - 0.00595(6.5 - \alpha_s{}^2)]b_o \tag{1.4}$$

$$c = [0.2711 + 0.01858(2.5 - \alpha_s{}^2)]c_o \tag{1.5}$$

Where α_s is the altitude of the observer in kilometers. The correction factors a_o, b_o and c_o are given for four climate types in the flowing table.

Table 1.1: Correction factors for four climate types (Hottel, 1976).

Climate type	a_0	b_0	c_0
Tropical	0.95	0.98	1.02
Midlatitude summer	0.97	0.99	1.02
Subarctic summer	0.99	0.99	1.01
Midlatitude winter	1.03	1.01	1.00

On other hand, (Kreith and Kreider, 1978) have described the atmospheric transmittance for beam radiation by the following empirical relationship.

$$\tau_b = 0.56[\exp(-0.65m) + (\exp(-0.095m)] \quad (1.6)$$

Where m is the air mass of the atmosphere.

Direct radiation (DNI): Direct radiation as described in figure 1.3, is the amount of solar radiation received at any place on the earth directly from the sun without any disturbances. In practical terms, this is the radiation which creates sharp shadows of the subjects. There is no interference by dust, gas, and cloud or any other intermediate material on the direct solar radiation. Hence, the terrestrial solar radiation on a horizontal plane can be estimated as (Hottel, 1976):

$$DNI = \tau_b I_{so} \cos(\theta_z) \quad (1.7)$$

Where I_{so} and DNI are the extraterrestrial and terrestrial intensities of direct radiation.

As shown in figure1.3, only the direct normal irradiation can be collected by the solar concentrators.

Diffuse radiation (I_d): the solar radiation component which has been scattered by the atmosphere.

Terrestrial solar radiation (I_T): the sum of the beam and diffuse radiation at the surface of the earth is called terrestrial or global radiation. Its value at any location is roughly proportional to direct solar radiation, and varies with the geometry of the receiving surface. The other components, such as diffuse radiation, vary only slightly from slope to slope within a small area and the variations can be linked to slope gradient (Williams et al., 1972).

$$I_T = DNI + I_d \tag{1.8}$$

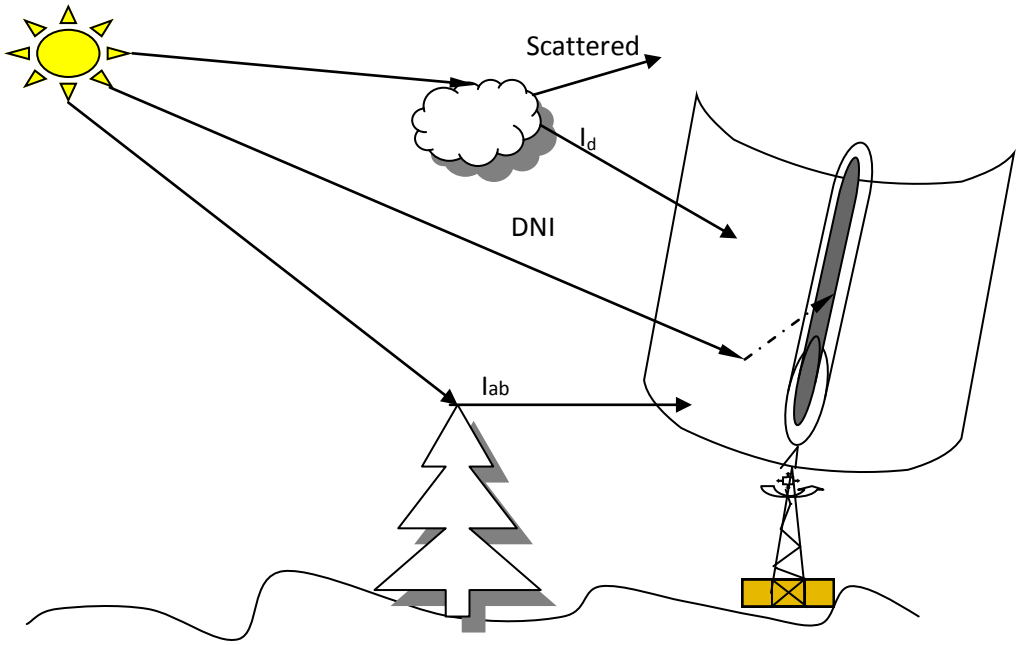

Figure 1.3: Terrestrial solar radiations.

1.1.2 Solar geometry and earth angle

The geometric relationship between the sun and the earth can be described by the latitude of the site, the true solar time, the angle between the sun and the earth, and the altitude and azimuth angles of the sun. It is also necessary to know the relation between the local standard time and the solar time.

Solar time: is the time based on apparent angular motion of the sun across the sky. Solar noon is the time where the sun crosses the meridian of the observer. There is a difference between clock time and solar time which varies at any instant depending on the east-west displacement. The relation between the local standard time and the solar time is given by (Duffie and Beckman, 1991).

$$\text{solar time} = \text{standard time} + 4(L_{st} - L_{loc}) + E \quad (1.9)$$

Where L_{st} , L_{loc} is, respectively, the standard meridian for the local time zone and the longitude of the location and E is the equation of time.

Equation of Time (E): this equation takes into account the perturbations in the earth's rate of rotation which affect the time the sun crosses the absorber meridian. The equation of time shown in figure 1.4 is determined by the following formulation (Spencer, 1972):

$$E = 229.2(75\ 10^{-6} + 186\ 10^{-6} \sin B - 0.03207 \sin B - 0.014615 \sin 2B - 0.04089 \sin 2B) \quad (1.10)$$

$$\text{Where: } B = (n_j - 1)360/365 \quad (1.11)$$

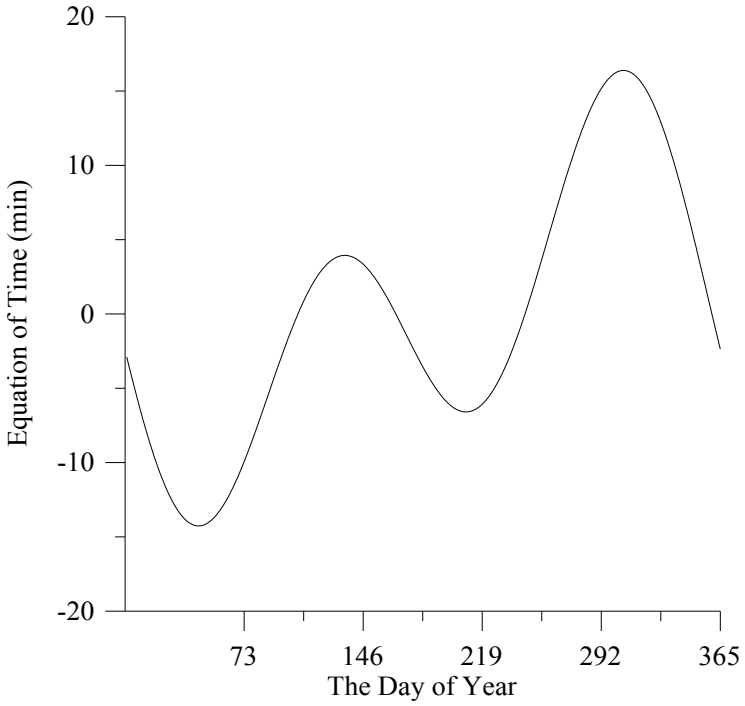

Figure1.4: The equation of time as a function of the time of year.

Hour angle (ω): the angular displacement of the sun east or west of the local meridian due to rotation of the earth on its axis at 15 degrees per hour angle. It express the time of the day with respect to the solar noon. It can be expressed by:

$$\omega = 15^{\circ}(\text{solar time} - 12) \quad (1.12)$$

Earth's Eccentricity (ε): It is desirable to have the distance and the earth's eccentricity in mathematical forms for simple calculations. Although a number of such forms are available of varying complexities, it is better to have simple and manageable expressions such as the one suggested by (Duffie and Beckman, 1991), who gave the eccentricity, ε, correction factor of the earth's orbit as:

$$\varepsilon = 1 + 0.033\cos\left(360\ n_j/365\right)] \tag{1.13}$$

The average distance between the sun and the earth is R = 150×10^6 km. Due to the eccentricity of the earth's orbit, the distance varies by 1.7%.

Declination angle(δ): The angle between the earth–sun line and the equatorial plane is called the declination angle which changes with the date and it is independent of the location. The declination is maximum 23°45'/minimum -23°45' on the summer/winter solstice and 0° on the equinoxes as shown in figure 1.5.

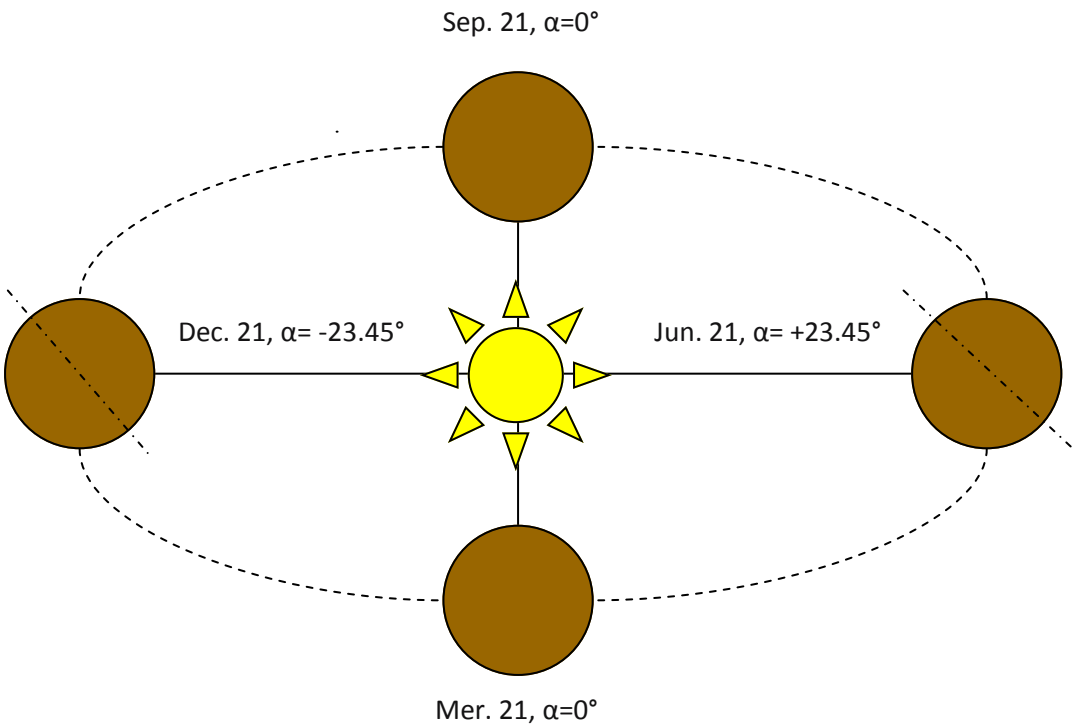

Figure 1.5: The declination angle.

The declination angle can be calculated as (Cooper, 1969):

$$\delta = 23.45\sin(360(284 + nj)/365) \quad (1.14)$$

It is also possible to consider the following expression for the accurate calculations of the declination angle in radians (Spencer, 1972):

$$\delta = 0.006918 - 0.399912\ \cos B + 0.07257\ \sin B - 0.006758\ \cos 2B + 0.000907\ \sin 2B - 0.002697\ \cos 3B + 0.00148 \sin 3B \quad (1.15)$$

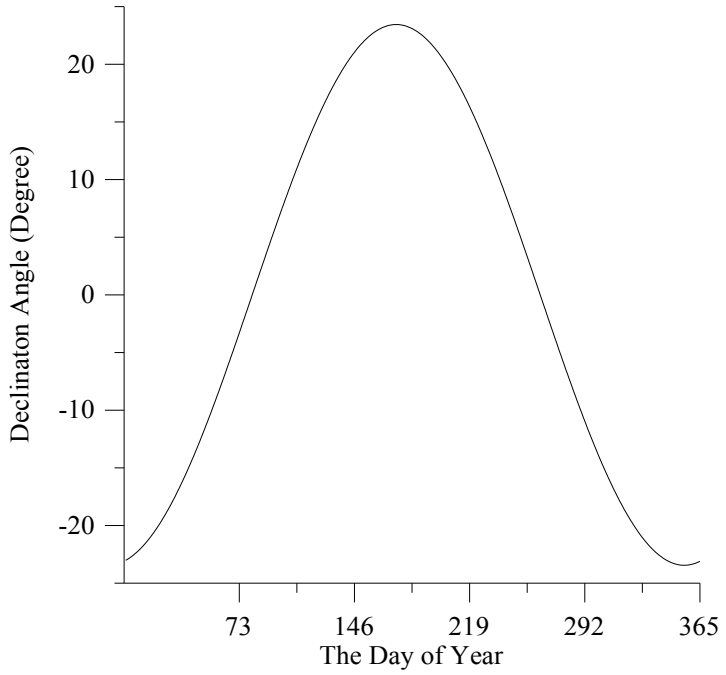

Figure1.6: Variation of extraterrestrial radiation with time of year.

1.1.3 Geographic locations

The basic angles that are necessary in the definition of the geographic locations are latitude and longitude.

Latitude (Φ): is the angular distance measured along a meridian from the equator (north or south) to a point on the earth's surface. Any location towards the north (south) has positive (negative) latitude with maximum (minimum) degrees as +90° (−90°) in the north (south) pole.

Longitude (L_{loc}): is the angular distance measured from the prime (solar noon) meridian through Greenwich west or east to a point on the earth's surface. Any location west (east) of the prime meridian is positive (negative) location.

1.1.4 Sun position in the sky

The position of the sun can be calculated for any location and any time. Figure 1.7 represents the angle to describe the position of the sun in the sky. Angles are described in the following way:

Solar altitude angle (α_s): it is the angle between the projection of the sun's rays on the horizontal plane and the direction of the sun rays (the complement angle of the zenith angle).

Solar zenith angle (θ_z): is the angle between the vertical and the line connecting to the sun. **Solar azimuth angle (γ_s)**: it is the angular displacement from the south of the projection of beam radiation on the horizontal plane.

Sunrise and sunset of the sun: the sunrise and sunset times at for any date and location can be calculated, respectively, from the following equations.

$$Sr = 12 - (\omega_s/15) \quad (1.16)$$

$$Ss = 12 + (\omega_s/15) \quad (1.17)$$

Where, ωs, is the sunset hour angle in degrees. It is given by (Duffie and Beckman, 1991):

$$\omega_s = \cos^{-1}[-\tan(\phi)\tan(\delta)] \quad (1.18)$$

Length of day: The number of daylight hours L_d can be calculated from the hour angle, since the hour angle changes by 15° every hour. The factor 2 results from taking into consideration morning and afternoon hours.

$$L_d = (2/15°)\arccos[\tan(\phi)\tan(\delta)] \quad (1.19)$$

1.1.5 Angles incidence on a plane

Angles describing the position of the surface in relation to the sun's rays and the earth are defined in this section and described by the figure 1.7.

Slop of the surface (β): is the angle between the plane of the surface and the horizontal plane.

Surface azimuth angle (γ): is the angle made in the horizontal plane between the line due south and the projection of the normal to the surface on the horizontal plane. $-180° < \gamma < +180°$

Angle of incidence (θ): is the angle between the beam radiation on a surface and the normal to that surface.

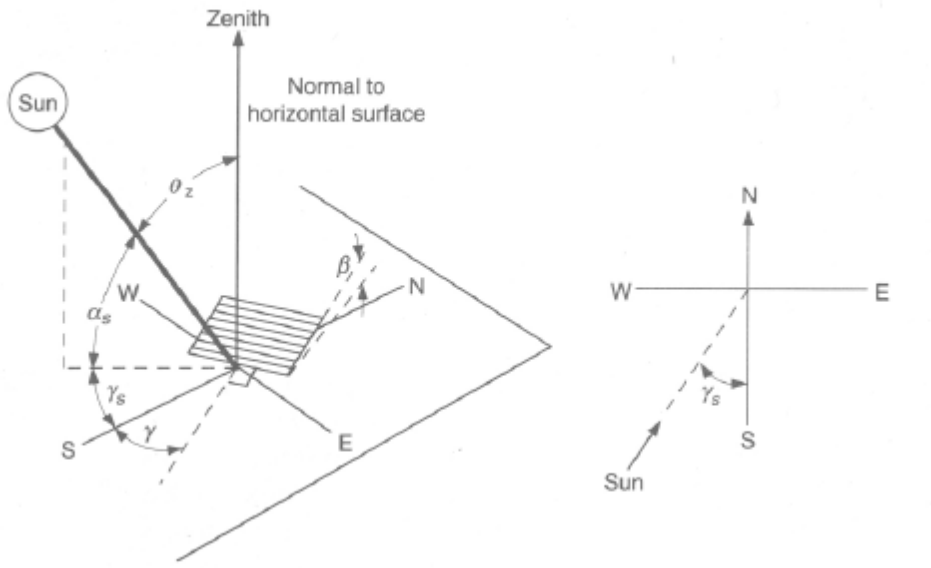

Figure 1.7 Solar angles (Duffie and Beckman, 1991).

The relation between the angle of incidence, the solar position angles is given by (Duffie and Beckman, 1991):

$$\cos(\theta) = \sin(\delta)\sin(\phi)\cos(\beta) - \sin(\delta)\cos(\phi)\sin(\beta)\cos(\gamma) + \cos(\delta)\cos(\phi)\cos(\omega)\cos(\beta) + \cos(\delta)\sin(\phi)\sin(\beta)\cos(\omega)\cos(\gamma) + \sin(\omega)\sin(\beta)\sin(\gamma)\cos(\delta) \quad (1.20)$$

For horizontal surface β=0°, the incidence angle equal to the zenith angle.

$$\cos(\theta_z) = \cos(\delta)\cos(\phi)\cos(\omega) + \sin(\delta)\sin(\phi) \quad (1.21)$$

1.1.6 Solar angles for tracking parabolic trough collector

Parabolic trough concentrators track the sun by moving prescribed ways to minimize the angle of incidence of beam radiation on their parabola and thus maximize the useful energy. Hence, the angle of incidence and the surface azimuth angle are needed. Tracking system can drive the collector to rotate around a single axis or around two axes. For parabolic through collectors, horizontal east-west and north-south axes are usually used.

Horizontal east-west rotation axis: for collectors rotating about a horizontal east-west axis with continuous adjustment to minimize the angle of incidence.

$$\cos(\theta) = [1 - \cos^2(\delta)\sin^2(\omega)]^{0.5} \quad (1.22)$$

This mode tracks the sun's position to achieve the optimum slope angle for the collector's aperture. The slope angle is given by (Duffie and Beckman, 1991).

$$\tan(\beta) = \tan(\theta_z)\left|\cos(\gamma_s)\right| \quad (1.23)$$

Horizontal north-south rotation axis: for collectors rotated about a horizontal north-south axis with continuous adjustment to minimize the angle of incidence. The employed control system in the ISCCS of Hassi R'Mel tracks the sun's position by this mode, to achieve the optimum slope angle for the collector's aperture. The optimum angle is given by (Alrobaei, 1998):

$$\beta_{opt} = \tan^{-1}[\sin(\omega)\cos(\delta)/\cos(\theta_z)] \quad (1.24)$$

The angle of incidence can be expressed by:

$$\cos(\theta) = \sin(\delta)\sin(\beta)\sin(\phi) + \cos(\delta)\cos(\phi)\cos(\omega)\cos(\beta) + \sin(\beta)\cos(\delta)\sin(\omega) \quad (1.25)$$

(Alrobaei, 1998) assumed that the aperture turns towards the east before noon (γ =-90°) and turns towards the west after midday (γ =+90°). At midday (ω =0°) the collector aperture is in horizontal position ($\boldsymbol{\gamma}$ =0°).

The slop angle can also given be by the following expression (Duffie and Beckman, 1991):

$$\tan(\beta) = \tan(\theta_z)\left|\cos(\gamma - \gamma_s)\right| \quad (1.26)$$

In this case the incidence angle is:

$$\cos(\theta) = [\cos(\theta_z)^2 + \cos(\delta)^2 \sin(\omega)^2]^{1/2} \quad (1.27)$$

The surface azimuth angle will be +90° or -90° depending on the sign of azimuth angle. i.e.

if $\gamma_s > 0°, \gamma = +90°$

if $\gamma_s < 0°, \gamma = -90°$

1.2 Parabolic through concentrator

Parabolic trough concentrator (PTC) will focus radiation on a receiver much smaller than the reflector. A PTC, like the one represented in the following figure, is basically made up of a parabolic trough shaped mirror that reflects direct solar radiation, concentrating it onto a receiver tube located in the focal line of the parabola. Concentration of the direct solar radiation reduces the absorber surface area with respect to the collector aperture area and thus significantly reduces the overall thermal losses. The concentrated radiation heats the heat transfer fluid circulating through the receiver tube, thus transforming the solar radiation into thermal energy in the form of the sensible heat of the HTF. This section treats the geometry, optical and thermal performances of these collectors.

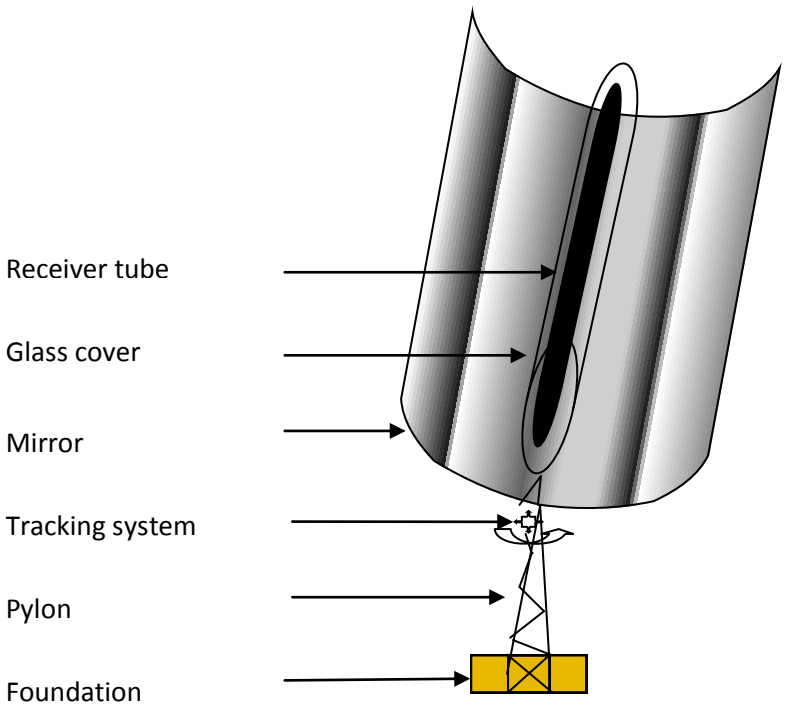

Figure 1.8: Typical parabolic through collector (PTC).

1.2.1 Collector's Geometric Elements

The three main factor of the design parameters required for a PTC are the geometric concentration ratio, the acceptance angle, and the rim angle. Consider the section of linear parabolic collector shown in figure 1.9. The length (l), the aperture (A_{ap}) and the height (H_p) of the parabola are given by the designer. Here are some definitions.

Focus length (f): by using the equation of the parabola the focus length is obtained.

$$f = y^2/4z \tag{1.28}$$

Geometric concentration ratio (C_c): is the ratio of the area of aperture to the area of the receiver.

$$Cc = A_{ap}/A_{abs} \tag{1.29}$$

Flux concentration ratio: is defined as the ratio of the average energy flux on the receiver to that on the aperture.

Acceptance angle ($2\theta_x$): is the angular range over which all or almost all rays are accepted without moving all or part of the collector. The half acceptance angle for the parabolic trough collector is as a function of the position (y) by:

$$\sin\theta_x = \mathrm{d}/2\mathrm{f}[1+\left(\frac{\mathrm{y}}{2\mathrm{f}}\right)^2] \tag{1.30}$$

For $Y = \pm y$ this formula gives θ_x, the largest angle for which all incident rays are accepted.

The half angle acceptance of the parabolic trough can be written also in terms of rim angle (φ_R) and concentration ratio (C_c).

$$\sin(\theta_x) = \sin(\varphi_R)/\pi Cc \tag{1.31}$$

The minimum practical acceptance angle is 0.53°, which is the average solid angle at which the sun sphere is seen from the earth. This means that any PTC with an acceptance angle smaller than 0.53° would always loose a fraction of the direct solar radiation. In fact, recommended acceptance angles for commercial PTCs are between 1° and 2°. Smaller angles would require very accurate sun-tracking system and frequent updating of the collector position, whereas higher values would lead to small concentration ratios and, therefore, lower working temperatures. Therefore, acceptance angle values between 1° and 2° are the most cost-effective (Alvarez and Zarza, 2007).

Rim angle (φ_R): is directly related to the concentrator arc length and a function of the parabola focal distance and aperture width (Duffie and Beckman, 1991):

$$\tan(\varphi_R) = 8(\frac{\mathrm{f}}{A_{\mathrm{ap}}})/[16\left(\frac{\mathrm{f}}{A_{\mathrm{ap}}}\right)^2 - 1] \tag{1.32}$$

Usual values for rim angles in a PTC are between 70° and 110°. Smaller rim angles are not advisable because they reduce the aperture surface. Rim angles over 110° are not cost-effective because they increase the total reflecting surface without effectively increasing the aperture width.

End effect (A_{loss}): is a collector geometrical end loss. (Rabl, 1985) gives an example of an end effect for receivers that are the same length as the reflector.

$$A_{loss} = 1 - [f/L(1 + \left(\frac{A_{ap}{}^2}{48f^2}\right) \tan\theta] \quad (1.33)$$

Absorber diameter (d): the minimum size of receivers centred at the focal line to intercept all of the reflected radiation from specular parabolic reflectors of perfect parabolic through collectors can be calculated as (Duffie and Beckman, 1991):

$$d_{abs} = A_{ap} \sin(0.267) / \sin(\varphi_R) \quad (1.34)$$

On the other hand, the diameter for imperfect parabolic through collectors can be described by the dispersion angle ά as:

$$d_{abs} = A_{ap} \sin(0.267 + (\acute{\alpha}/2)) / \sin(\varphi_R) \quad (1.35)$$

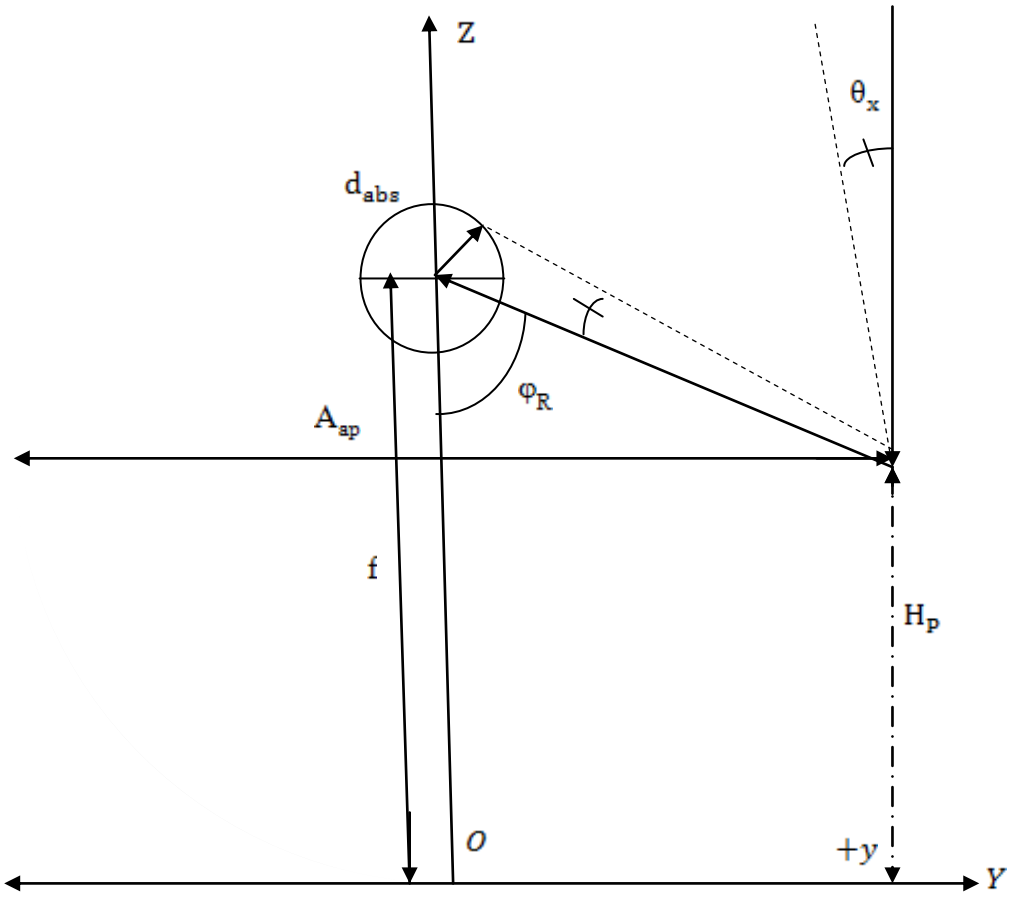

Figure 1.9: Geometric elements of PTC.

1.2.2 Collector's optical performances

The optical efficiency (η_{opt}): It is defined as the fraction of the solar radiation incident on the aperture of the collector, which is absorbed at the surface of the absorber tube. It is the multiplication of four parameters (reflectivity, intercept factor, glass transmissivity, and absorptivity of the steel pipe) when the incidence angle on the aperture plane is 0°.

$$\eta_{opt,0^{\circ}} = \rho \times \tau \times \alpha \times \vartheta \tag{1.36}$$

Where: ρ is the reflectivity of the collector reflecting surface, τ is the transmissivity of the glass tube, α is the absorptivity of the absorber selective coating and ϑ is the intercept factor.

intercept factor (ϑ) : is the fraction of the direct solar radiation reflected by the mirrors which does not reach the glass cover of the absorber tube due to either microscopic imperfections of the reflectors or macroscopic shape errors in the parabolic trough concentrators.

Absorptivity (α): absorptivity of the absorber selective coating is the amount of energy absorbed by the steel absorber pipe, compared with the total radiation reaching the outer wall of the steel pipe.

Reflectivity (ρ): in general less than one. It value continuously decreases after washing the mirrors. Hence, only a fraction of the incident radiation is reflected towards the receiver tube.

Transmissivity (τ): The ratio between the radiation going through the glass tube and the total incident radiation on this tube.

The incidence angle modifier $K(\theta)$: It is necessary to use the incident angle modifier which gives the error in the concentration counter due to using the sun tracking system. The incidence angle modifier represent the effect of the incidence angle on the optical efficiency and useful aperture area of a PTC because this parameter includes all optical and geometric losses due to an incidence angle greater than 0° i.e. collector end losses, collector center losses, blocking losses due to absorber tube supports, angle dependence of the intercept factor, angle dependence of reflectivity, transmissivity, and absorptivity. In the present research, the incident angle modifier is assumed that it is similar to the LS3 collector (Alvarez and Zarza, 2007).

$$\mathrm{K}(\theta) = 1 - 2.23073\ 10^{-4}(\theta) - 1.1\ 10^{-4}(\theta)^2 + 3.185\ 10^{-6}(\theta)^3 - 4.855\ \ 10^{-8}(\theta)^4 \tag{1.37}$$

1.2.3 Collector's thermal performances

A typical parabolic trough collector is basically made up of a parabolic trough shaped mirror that reflects direct solar radiation, concentrating it onto a receiver tube located in the focal line of the parabola. The useful energy gained by this collector can be given as a function of absorber temperature (Alvarez and Zarza, 2007):

$$Q_c = A_c DNI \cos\theta \, \eta_{opt} K(\theta) - A_{abs} U_{abs} (T_{abs} - T_a) \quad (1.38)$$

Where: A_c is the collector aperture surface, A_{abs} is the absorber area, T_{abs} is the mean absorber pipe temperature and T_a is the ambient air temperature and U_{abs} is the absorber thermal loss coefficient.

The absorber temperature is evaluated by the following equation:

$$T_{abs}{}^4 = [(\alpha \, DNI \, C_c \frac{\eta_{opt}}{\sigma \varepsilon}) + T_a{}^4] \quad (1.39)$$

The heat loss coefficient depends on the absorber pipe temperature and is found experimentally by performing specific thermal loss tests with the solar collector operating at several temperatures within its typical working temperature range. Variation in the thermal loss coefficient versus the receiver pipe temperature can usually be expressed with a second order polynomial equation, with coefficients a, b, and c experimentally calculated:

$$U_{abs} = a + b(T_{abs} - T_a) + c(T_{abs} - T_a)^2 \quad (1.40)$$

The table below gives the values of coefficients a, b, and c that have been experimentally calculated by Ajona (1999) for LS-3 collectors installed at SEGS VIII and IX.

Table 1.2: Values of Coefficients a, b, and c for a LS-3 Collector. (Alvarez and Zarza, 2007)

T_{abs}(℃)	a	b	C
from 200 to 300	1.433242	-0.00566	0.000046
Up to 300	2.895474	-0.0164	0.000065

2. INTEGRATED SOLAR COMBINED CYCLE SYSTEM

2.1 What is ISCCS?

Integrated Solar Combined Cycle System (ISCCS) is a new design concept that integrates a parabolic trough solar field with a modern combined cycle power plant. This integration provides a great flexibility of management and control difficult to realize in the traditional solar power stations. The adjustment of the solar power station can be done by the flexibility of the gas turbines or by the solar concentrators. The ISCCS has generated much interest because it offers an innovative way to reduce cost and improve the overall solar to electric efficiency. This future power plant would operate at the combined cycle mode during non solar periods, and then the output would increase when solar energy is available. The initial concept was simply to increase the size of the steam turbine, use solar energy to generate steam, and use the waste heat from the gas turbine to preheat and superheat the steam.

A number of recent studies have looked at the best approaches for this integration. Most designs have looked at oversizing the steam turbine. ISCCS plants typically have very low solar contributions, on the order of 1% to 15% of annual output for a base load combined cycle plant. Nowadays no power plants from this kind have been built. The ISCCS under erection in Algeria is the proposed power plant in this project.

In this study, an ISCCS with simple pressure level is proposed. During sunny periods, one part of feed water is withdrawn from the heat recovery steam generator HRSG converted to saturated steam in the solar steam generator HSSG. This saturated steam is returned to the HRSG where it is mixed and superheated. At night and during cloudy periods the integrated solar combined cycle system operates as a combined cycle. A process flow diagram for proposed ISCCS is shown in Figure 2.1.

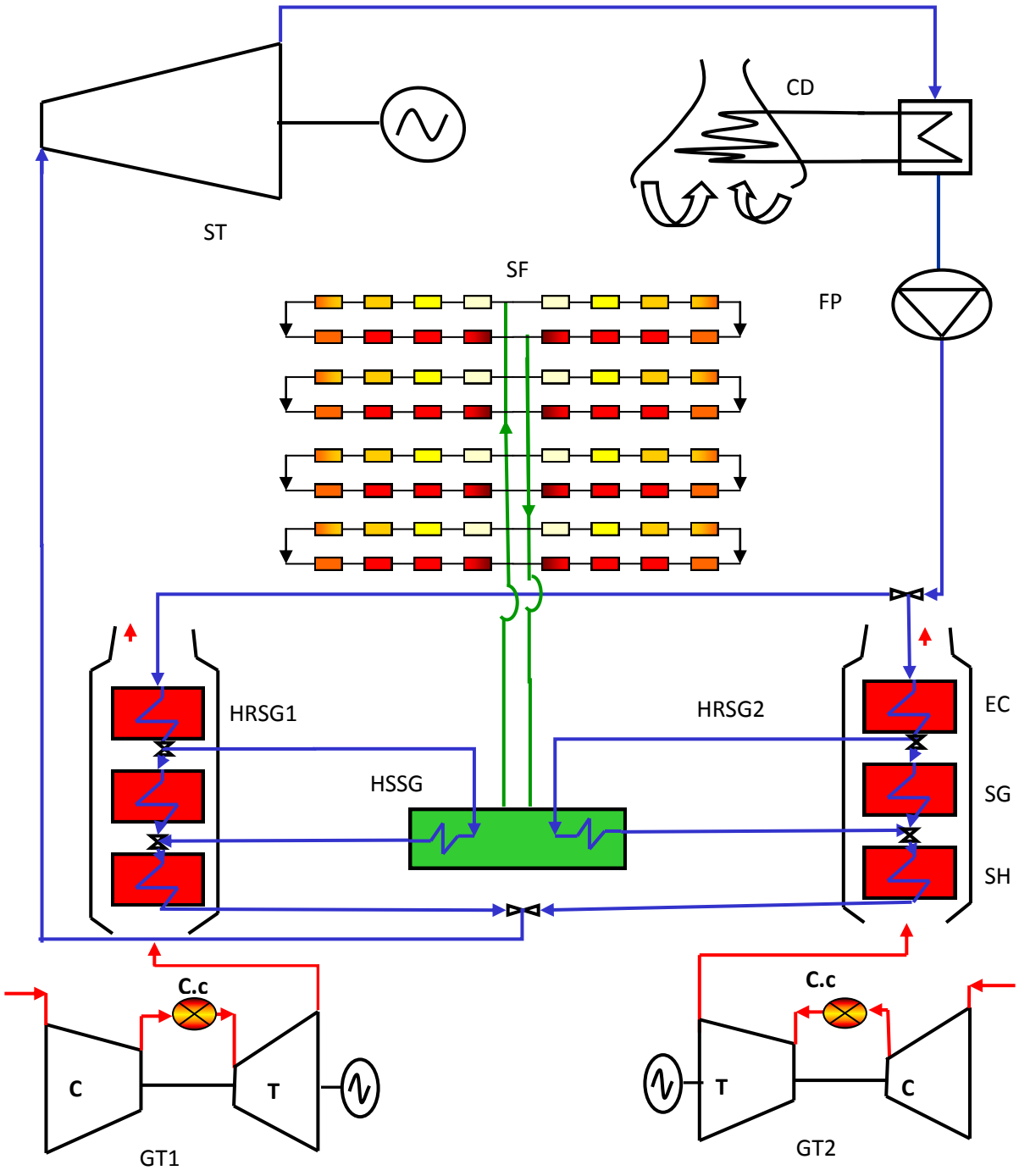

C: Axial compressor, C.c: Combustion chamber, CD: Air condenser, EC: Economiser, FP: Feed water pump, GT: Gas turbine unit, HRSG: Heat recovery steam generator, HSSG: Heat solar steam generator, SF: Solar filed, SG: Steam generator, SH: Superheater, ST: Steam turbine unit, T: Turbine section.

Figure 2.1: Integrated solar combined cycle system of Hassi R'mel, Algeria.

2.2 The solar field

The solar field of Hassi R'mel Desert is divided in two parts; both consist of a numerous parabolic trough collector (PTC), as shown in figure 2.2. Each parabolic trough collector has a linear parabolic shaped reflector that focuses the sun's direct beam radiation on a linear receiver located at the focus of the parabola. The collectors track the sun from east to west during the day to ensure that the sun is continuously focused on the linear receiver. A heat transfer fluid (HTF) is heated as it circulates through the receiver and returns to the solar heat exchanger to generate saturated steam.

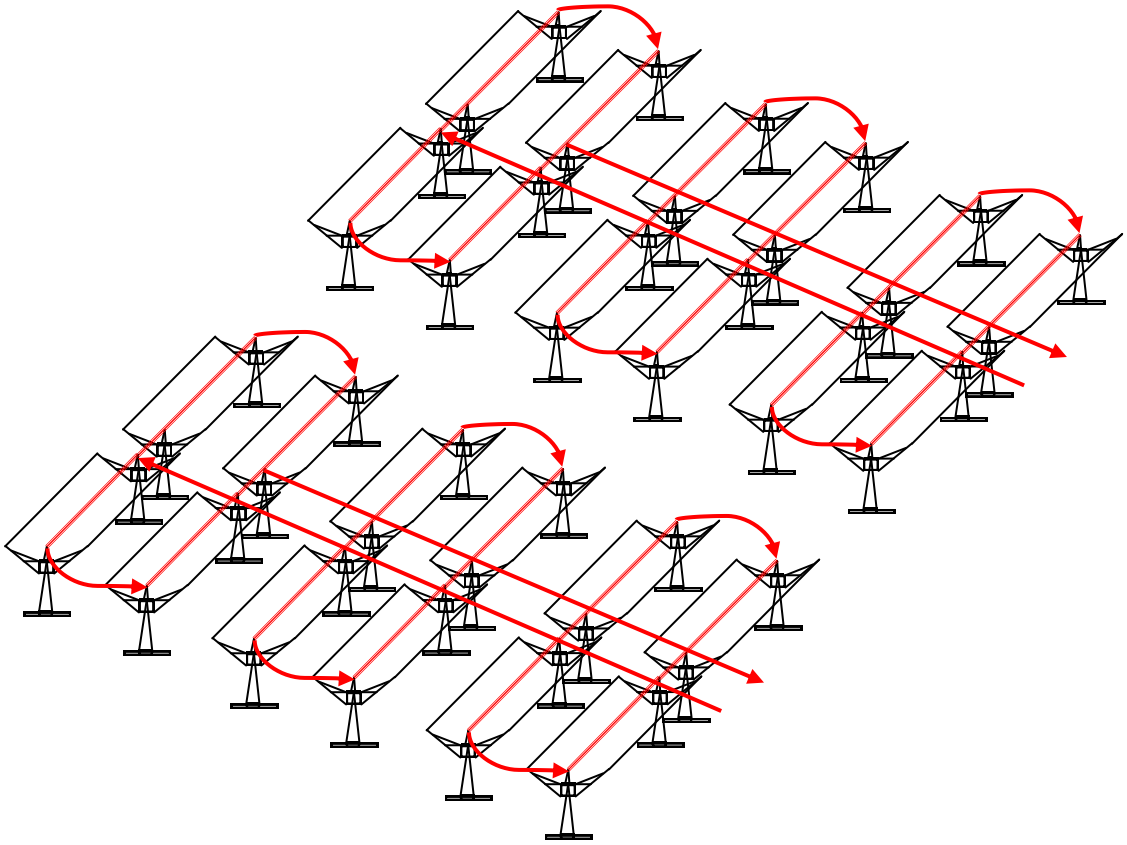

Figure 2.2: Solar fields of Hassi R'mel ISCCS.

The solar field's basic component is the parabolic trough collector (PTC). As shown in figure 2.3, each PTC is made up of parabolic reflectors (mirror), a metal support structure (pylon and support), a receiver tubes, glass cover and a tracking system that includes a drive, sensors and controls.

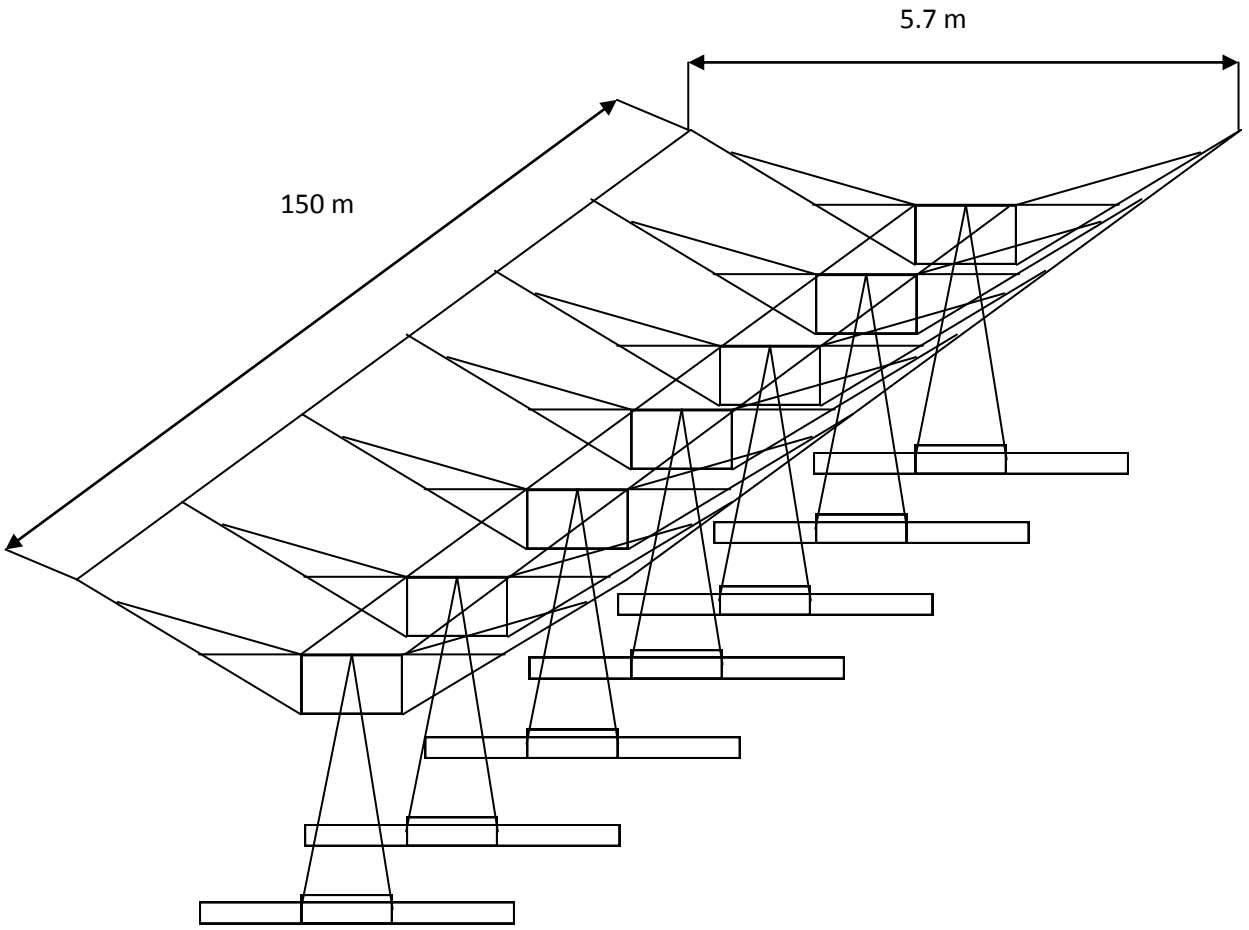

Figure 2.3: Euro Trough collector (ET150).

The Euro Trough (ET 150) collector which is used in the selected ISCCS of Hassi R'mel consists of identical 12 m long collector modules. Each module comprises 28 parabolic mirror panels (7 along the horizontal axis between pylons and 4 in a vertical cross-section). Each mirror is supported on the structure at four points on its backside. This permits the glass to bend within the range of its flexibility without effect on the focal point.

(ET 150) has less weight and less deformations of the collector structure due to dead weight and wind loading than the LS-3 collector. This reduces torsion and bending of the structure during operation and results in increased optical performance and wind resistance. The weight of the steel structure has been reduced about 14% as compared to the available design of the LS-3 collector (George Barakos, 2006).

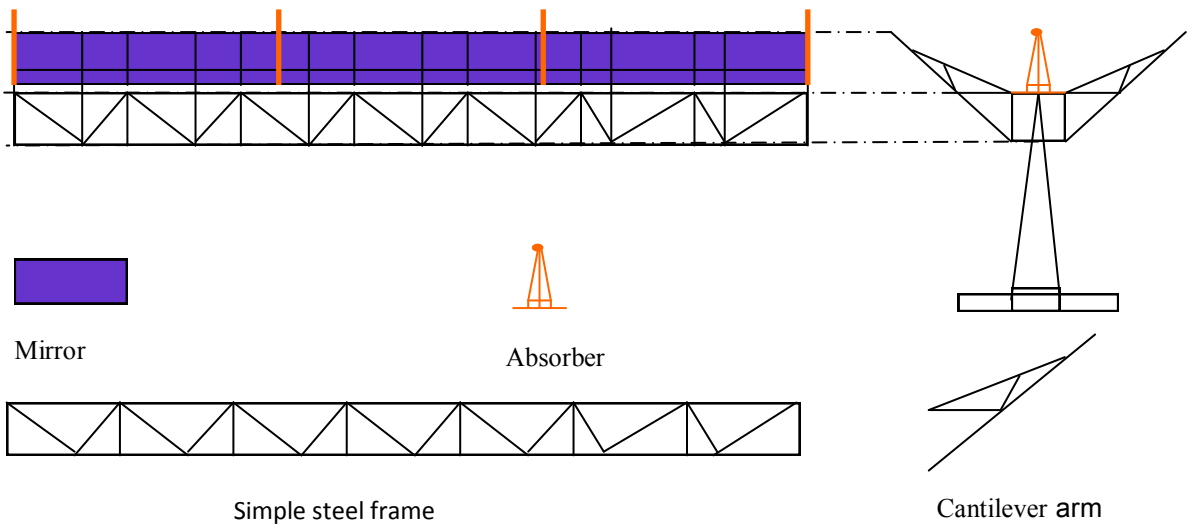

Figure 2.4: Euro Trough collector elements ET150

The mirrors are made from a low iron float glass with a transmissivity of 98% that is silvered on the back and then covered with several protective coatings. The mirrors are heated on accurate parabolic molds in special ovens to obtain the parabolic shape. Ceramic pads used for mounting the mirrors to the collector structure are attached with a special adhesive.

The heat collection element (HCE) consists of steel tube with a cermets selective surface, surrounded by an evacuated glass tube. The HCE incorporates glass-to-metal seals and metal bellows to achieve the vacuum tight enclosure. The vacuum enclosure serves primarily to protect the selective surface and to reduce heat losses at high operating temperatures.

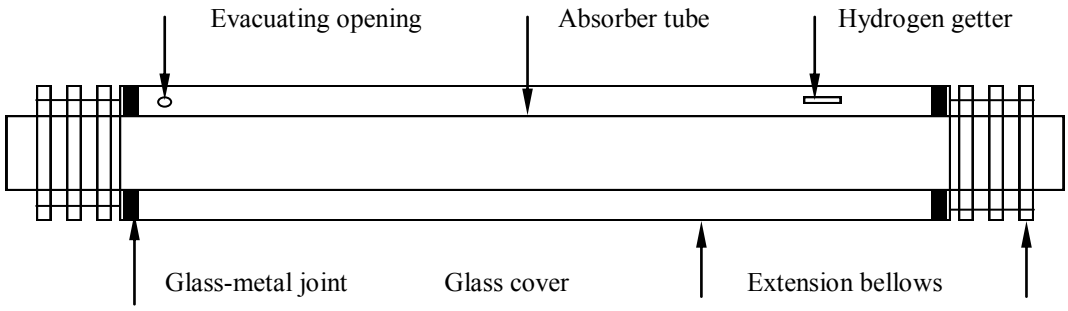

Figure 2.5: The Heat Collector Element (HCE).

The vacuum in the HCE is maintained at about 0.013 Pa. The outer glass cylinder has an antireflective coating on both surfaces to reduce reflective losses off the glass tube. Getters, metallic substances that are designed to absorb gas molecules, are installed in the vacuum space to absorb hydrogen and other gases that permeate into the vacuum space over time.

The Euro Trough collector is tracked with the sun during operation along their long axis with a hydraulic drive. The drive system consists of two hydraulic cylinders mounted on the central drive pylon. From a control box mounted on the drive pylon signal and power lines lead to the hydraulic unit, the rotational encoder, limit switches and temperature sensors. The tracking system developed for the Euro Trough collector is based on virtual tracking. The traditional sun tracking unit with sensors that detect the position of the sun has been replaced by a system based on calculation of the sun position using a mathematical algorithm. Comparing both sun and collector axes positions by an electronic device, an order is sent to the drive system, inducing tracking.

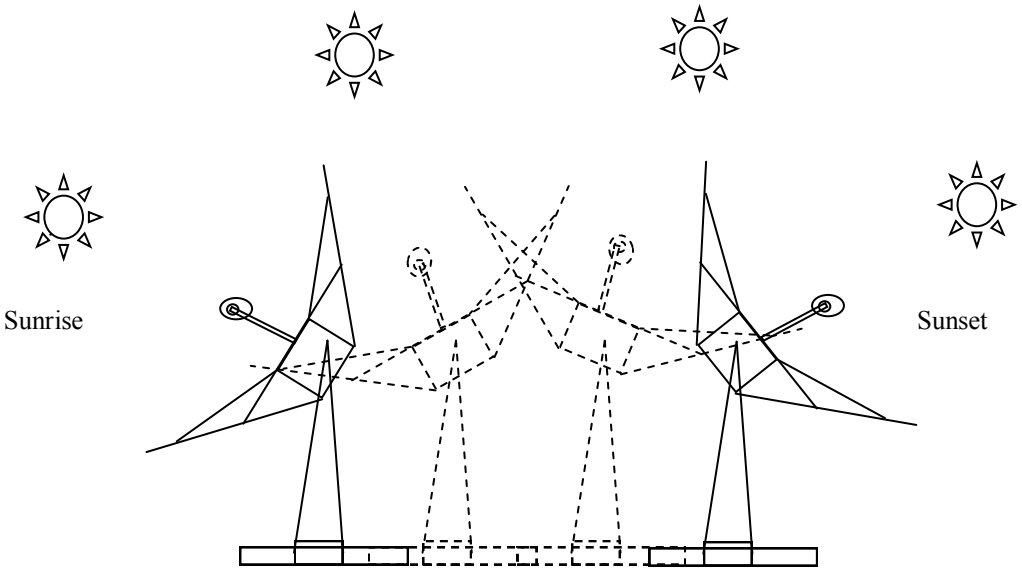

Figure 2.6: PTC track the sun from sunrise to sunset.

Tracking system can drive the collector to rotate around the horizontal north/south or east/west axis for tracking the sun as it moves through the sky during the day. The axis of rotation is at the collector center of mass to minimize the tracking power required. The drive system uses hydraulic rams to position the collector. A closed-loop tracking system relies on a sun sensor for the precise alignment required to focus the sun on the HCE during operation.

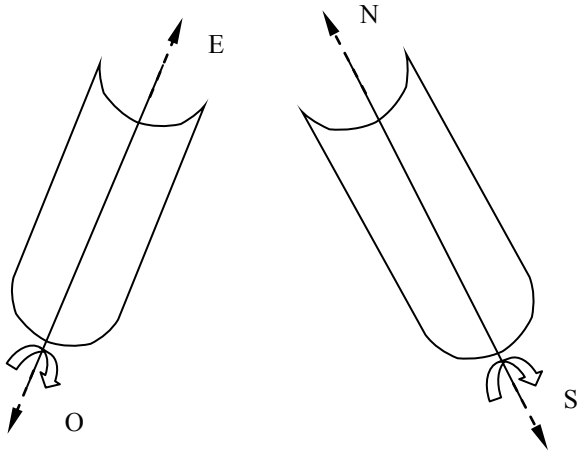

Figure 2.7: The appropriate rotate axis.

The most appropriate control system is in a north/south oriented rotation axis, where collectors are aligned on the north-south axis and collectors rotate from east to west tracking the sun's position. The control system continuously drives the collectors from east at sunrise to west at sunset.

The collectors are aligned in the North-South direction and are connected in a series to form long lines, which in their turn are connected in parallel for forming the solar field. The size of the solar field depends on the desired power and the outlet temperature. It can have several configurations according to the way in which the heat transfer fluid (HTF) is fed in. In all the cases, the piping of exit is the shortest possible to minimize the losses with environment. Three basic layouts which are usually used are direct-return, reverse-return, and center-feed. They are shown schematically in Figure 2.8.

The **direct return** piping configuration is the simplest and probably the most extensively used in small solar fields. Its main disadvantage is that there is a much greater pressure difference between the inlets in parallel rows, so that balancing valves must be used to keep the flow rates the same in each row. These valves cause a significant pressure drop at the beginning of the array, and thus their contribution to the total system pressure loss is also significant. The result is higher parasitic energy consumption than for the reverse return layout, where the fluid enters the collector array at the opposite end. Pipe headers with different diameters are used in this configuration to balance the array flow. The use of larger pipe headers also results in lower

parasitic power requirements, but these could be offset by increasing in initial investment costs and thermal energy losses.

The **reverse return** layout has an inherently more balanced flow. While balancing valves may still be required, the additional system pressure loss is much lower than in a direct return configuration(Alternatively, header pipes can be stepped down in size on the inlet side and stepped up on the outlet side to keep flow rate in the headers constant, thereby providing uniform flow).The extra length of piping at the solar field inlet is a disadvantage in the reverse return configuration because of the additional heat loss, although this greatly depends on the solar field inlet temperature. If this temperature is low, additional heat loss is negligible. Adding to pipe length, however, results in higher piping, insulation, and fluid inventory costs.

The **center feed** configuration is the most widely used layout for large solar fields. This is the selected layout in ISCCS of Hassi R'mel. As in the direct return design, pressure loss in the solar field is greater if balancing valves are installed at the row inlets. This layout minimizes the total amount of piping because there is no pipe running the length of the collector row. There is also direct access to each collector row without buried pipes.

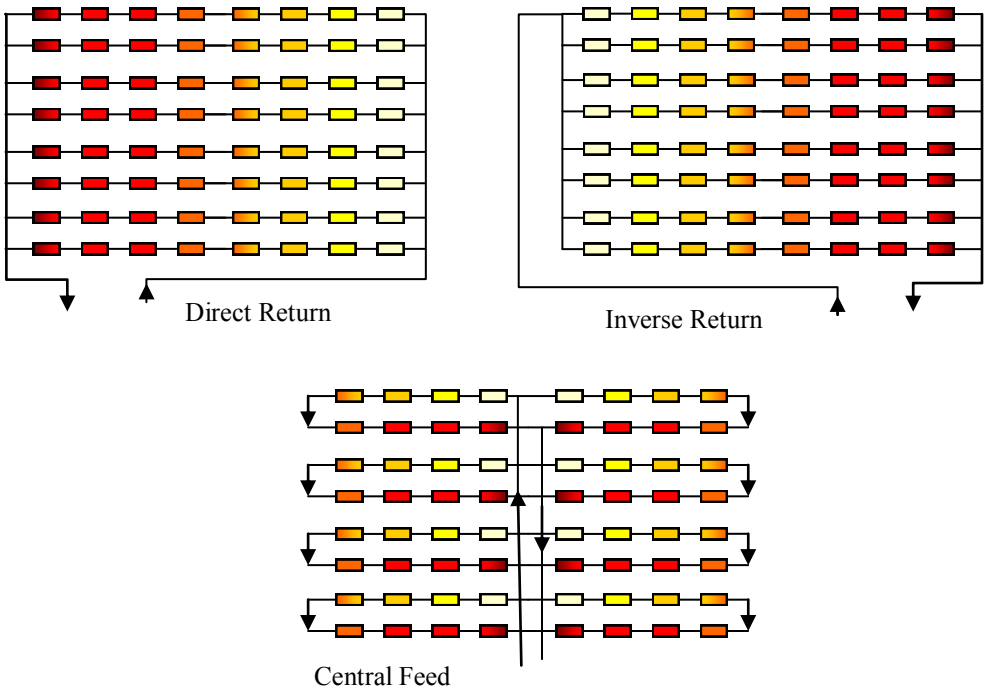

Figure 2.8: Solar field layouts for parabolic trough collectors.

2.3 Combined cycle

The combined cycle, like the one represented in figure 2.9, consists of two gas turbine (Brayton cycle), a steam turbine (Rankin cycle) and two heat recovery steam generator. The exhaust gases from the gas turbine unit flows through the heat recovery steam generator (HRSG) to generate and superheat steam which is driven to be expanded in a steam turbine.

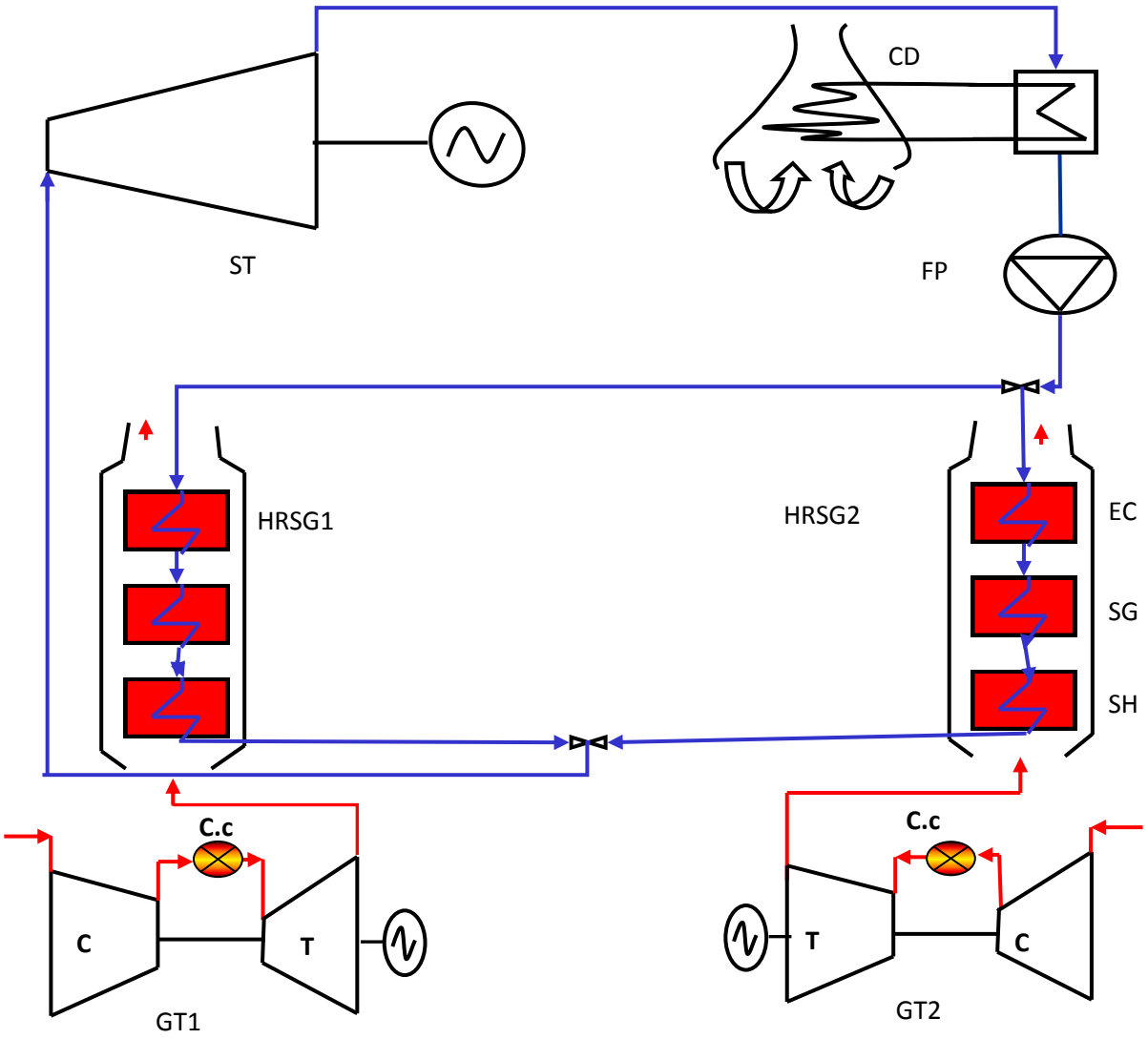

C: Axial compressor, C.c: Combustion chamber, CD: Air condenser, EC: Economiser, FP: Feed water pump, GT: Gas turbine unit, HRSG: Heat recovery steam generator, SG: Steam generator, SH: Superheater, ST: Steam turbine unit, T: Turbine section.

Figure 2.9: Combined cycle power plant.

2.3.1 Brayton cycle

The gas turbine is made up of three main parts which are a compressor, a combustion chamber and a turbine. First, the air is passed through the axial compressor intake, where it is compressed. Then, some of this is extracted for the internal cooling system of the turbine blades. The other part is flow through the combustion chamber where it is heated up. In the combustion chamber, fuel is burned with air at a constant pressure. Finally, the hot gases are expanded from the gas turbine inlet pressure to the ambient air pressure.

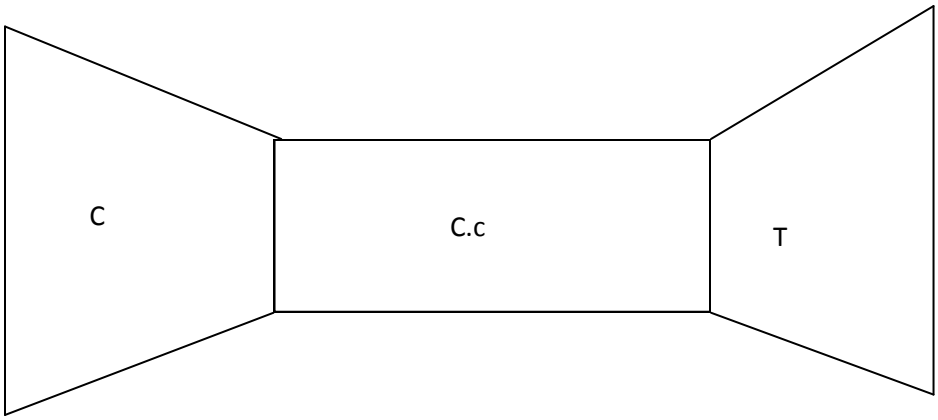

Figure 2.11: Principal parts of the gas turbine engine.

The gas turbine performance depends on the performance of three main parts. The Compression ratio, the combustion efficiency and turbine inlet temperature are important parameters for gas turbine analysis.

As shown in the following figure, the thermodynamic cycle of the ideal gas turbine, known as the ideal Brayton cycle, consists of four processes.

1. Isentropic compression;

2. Constant pressure heat addition in the combustion chamber;

3. Isentropic expansion;

4. Constant pressure heat rejection.

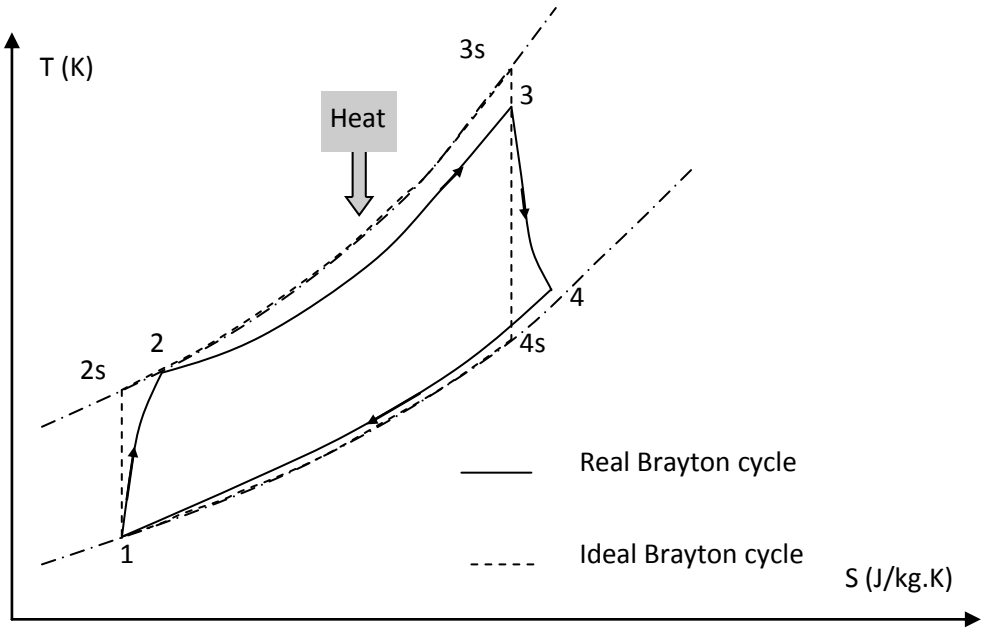

Figure 2.11: Gas turbine thermodynamic cycle.

The difference between ideal and real Brayton cycle represents the energy and the exergy losses including adiabatic compression, pressure drop within heat adding process and adiabatic expansion (more details in the following chapters).

2.3.2 Rankin cycle

The heat recovery steam generator of the Rankine cycle is a network of heat exchangers used to recover some heat from the exhaust gases of the gas turbines. It consists of three main sections, i.e. a superheater, an evaporator and an economiser. The HRSG function in the combined cycle is divided to three main processes: heating the feed water to increase the water temperature up to the saturated temperature, the evaporating process which includes converting the water into steam, and the superheating section which increases the steam temperature up to the desired state. Figure 2.12 shows the thermodynamic cycles of the gas turbine and the steam turbine in the CC.

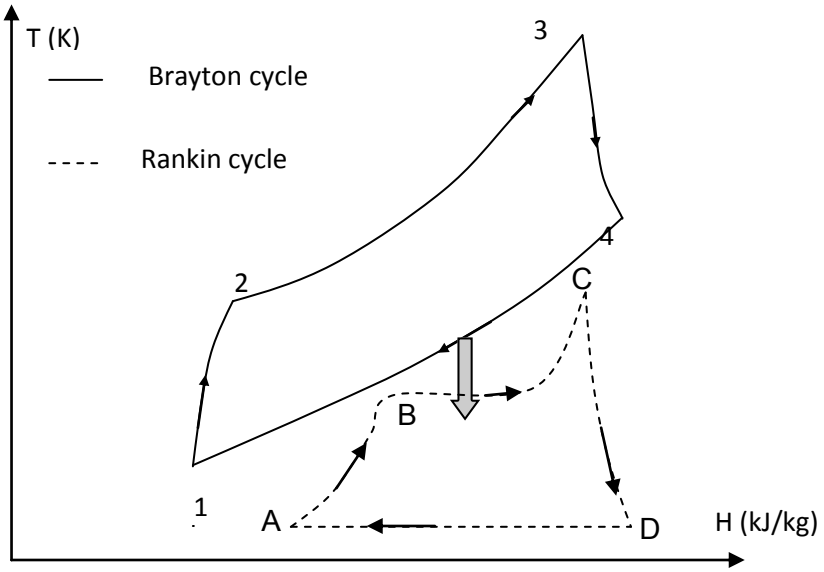

Figure 2.12: T (H) Diagram of a combined cycle power plant with simple pressure.

3. ISCCS THERMODYNAMIC ANALYSIS

3.1. Solar field analysis

To evaluate the thermal performances of the solar field, the variation of thermal energy and mass flow of the heat transfer fluid, the energy balance between solar radiations, heat absorption by HTF and heat losses are used.

The useful energy gained by the heat transfer fluid at the point of absorber can be given by equation (1.38).

The peak optical efficiency of the solar collector is obtained by equation (1.36).

The incidence angle modifier is given by equation (1.37).

The direct normal irradiation is estimated by Hottel method for clear sky. It is calculated by using the equation (1.7).

The incidence angle is determined by equation (1.27).

The heat loss coefficient can be estimated by using equation (1.40).

The absorber temperature T_{abs} can be obtained from equation (1.39).

The solar field performances are the useful solar energy, mass flow of the HTF and the solar field efficiency.

The total useful energy gained by the heat transfer fluid in the solar is:

$$Q_{SF} = N_L . C_L . Q_C \quad (3.1)$$

Where: C_L, N_L are, respectively, the number of collectors in each row and the numbers of line in the solar field.

The mass flow can be given by:

$$m_{sf} = Q_{SF} / C_{pHTF} . \Delta T_{sf} \quad (3.2)$$

The solar field efficiency is the ratio of the net useful energy gained by the heat transfer fluid in the solar field and the total quantity of solar beam which reaches the mirrors of the solar field.

$$\mathcal{E}_{SF} = Q_{SF} / DNI \,.\, A_c \,.\, N_L \,.\, C_L \quad (3.3)$$

Note: the heat transfer fluid which is proposed is named THERMONOL VP-1. Some physical proprieties formulae of this synthetic oil as a function of the temperature are experimentally obtained.

Density (kg/m^3):

$$\rho_{VP\_1} = -0.90797\, T + 0.00078116\, T^2 - 2.367\, 10^{-6}\, T^3 + 1083.25 \quad (3.4)$$

Heat capacity (kj/kg.K):

$$Cp_{VP-1} = 0.002414\, T + 5.9591\, 10^{-6} T^2 - 2.9879.\, 10^{-8} T^3 + 4.4172.\, 10^{-11} T^4 + 1.498 \quad (3.5)$$

Latent heat vaporisation (kj/kg):

$$L_{VP-1} = -0.528933\, T - 7.50103\, 10^{-5} T^2 + 1.5622\, 10^{-6} T^3 - 3.771\, 10^{-9} T^4 + 425.18 \quad (3.6)$$

Thermal conductivity (W/m.K);

$$\lambda_{VP-1} = -8.19477\, 10^{-5} T - 1.9228\, 10^{-7} T^2 + 2.503\, 10^{-11} T^3 - 7.297\, 10^{-15} T^4 + 0.137743 \quad (3.7)$$

3.2. Gas turbine thermodynamic analysis

In the ISCCS power plant the main purpose of analysing the gas turbine unit is to evaluate the waste energy within the exhaust gases. Estimating the exhaust gases mass flow and its temperature is the main goal of this section. The procedure to achieve this goal is to evaluate the compressor, the combustion chamber and turbine performances.

The ideal gas turbine thermodynamic cycle is known as the Brayton-Joule cycle which is described by four processes: isentropic compression, constant pressure heat addition, isentropic expansion and constant pressure heat release is described in figure 3.2.

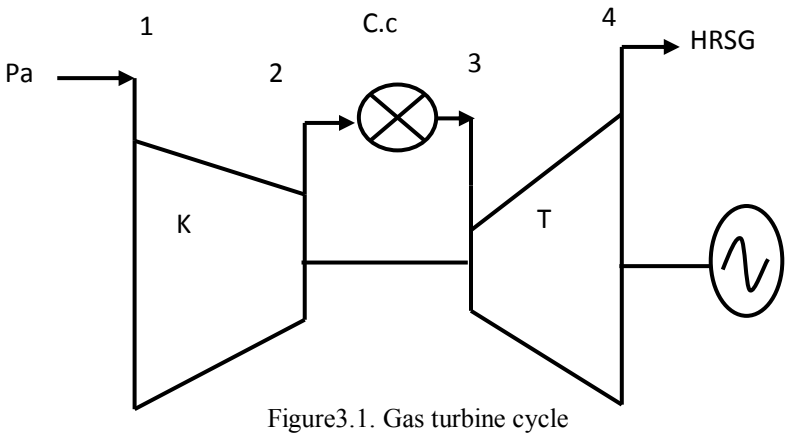

Figure3.1. Gas turbine cycle

As represented in figure 2.11, subscripts 1, 2, 3 and 4 refer to the states of air and gas at different stages of real gas turbine cycle; however superscript 1, 2s, 3s and 4s refer to ideal cycle.

The axial compressor:

As the air is passed through the compressor's intake some pressure losses occur. So the pressure at the first stage is less than the pressure at the compressor intake entrance. Experiments show that this loss can be evaluated as:

$$dP_1 = P_a - P_1 \tag{3.8}$$

Where dP_1 are the hydraulic losses due to air flow through the compressor intake. Its value is 0.005 Bars (Siemens Corporation). So that pressure at the first compressor stage is equal to:

$$P_1 = P_a - dP_1 \tag{3.9}$$

The air temperature at the compressor entrance T_1 is assumed to be equal to the ambient temperature.

The compressor pressure ratio is:

$$\sigma_k = \frac{P_2}{P_1} \tag{3.10}$$

The following relation provides the compressor exit air temperature for isentropic process.

$$T_{2s} = T_1(\sigma_k)^{\frac{\gamma_k - 1}{\gamma_k}} \quad (3.11)$$

The compressor isentropic efficiency is equal to:

$$\eta_s^k = \frac{(\frac{P_2}{P_1})^{\frac{\gamma_k - 1}{\gamma_k}} - 1}{(\frac{P_2}{P_1})^{\frac{\gamma_k - 1}{\gamma_k \eta_p^k}} - 1} \quad (3.12)$$

It is also can be given by:

$$\eta_s^k = \frac{h_{2s} - h_1}{h_2 - h_1} \quad (3.13)$$

Thereby:

$$h_2 = h_1 + \frac{h_{2s} - h_1}{\eta_s^k} \quad (3.14)$$

Where η_s^k compressor isentropic efficiency, η_p^k is the compressor polytropic efficiency and γ_k is the specific heat ratio.

The specific heat ratio is determined by the following equation:

$$\gamma_k{}' = 1/[1 - \left(\frac{r_k}{Cp_k}\right)] \quad (3.15)$$

Where: Cp_k is the average specific heat at constant pressure in the compressor and r_k is the air constant. An experimental correlation is used to estimate the specific heat at constant pressure.

$$Cp = a + bT + cT^2 + dT^3 \quad (3.16)$$

With a, b, c, d are constants specific for air

Constants specific for air	a	b (/10^{-2})	c(/10^{-5})	D (/10^{-9})
Values	28.11	0.19	0.48	1.97

The first value of γ_k is assumed to be equal to the specific heat ratio of air at ambient temperature, then a new value for the specific heat ratio is calculated from equation (3.15) . An iteration process is carried out until a desired accuracy is met $|\gamma_k{}' - \gamma_k| < 10^{-5}$.

Consequently the actual conditions at the end of the compression process are achieved.

The combustion chamber:

After the compression process some air is extracted for the air cooling system. The extracted air is used for the internal cooling system of the turbine blades.

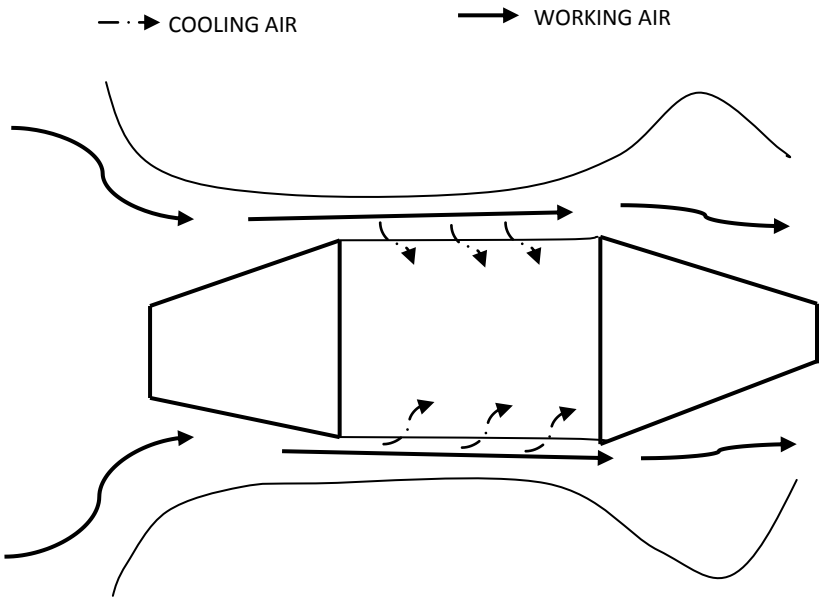

Figure 3.3: Air flow into the gas turbine.

An experimental correlation is used to estimate the relative mass flow for cooling air to the entire air mass flow in the gas turbine (Alrobaei, 1998).

$$m_R = [0.02 + 0.00032(T_3 - T_b)] \quad (3.17)$$

Where m_R is the relative air mass flow rate for blades cooling and T_b is the mean temperature of turbine blades, the value of this latter varies from 750 °C to 850 °C (Alrobaei, 1998).

The other part of the compression air flows through the combustion chamber where it is heat up. As well as, its pressure drops down. Hence, the pressure in the combustion chamber outlet is:

$$P_3 = P_2(1 - dP_2) \tag{3.18}$$

Where $dP_2$is the hydraulic losses coefficient in the combustion chamber, its typical value is 0.015 to 0.025 (Alrobaei, 1998).

Assuming the gas turbine has a cans annular reverse flow type combustion chamber like the one represented in figure (3.4). The energy balance of the combustion chamber can be given by the following equation:

$$(1 - m_R)C_{P2}T_2 + m_f Q_{cv}\eta_{cc} = (1 - m_R + m_f)C_{P3}T_3 \tag{3.19}$$

Where m_f fuel mass flow rate and η_{cc} is the combustion chamber efficiency, its typical value is 0.9 to 0.98, Q_{cv} is the Fuel calorific value and T_2 , T_3 are respectively, the temperature in the compressor exit and the combustion chamber exit.

From the equation above the fuel mass flow rate can be given by:

$$m_f = (1 - m_R)(C_{P3}T_3 - C_{P2}T_2)/[(Q_{cv}.\eta_{cc}) - C_{P3}T_3] \tag{3.20}$$

Assuming that the air to fuel ratio for combustion $\propto_o$=15 kg air/kg fuel. The excess air coefficient is given by:

$$\propto_a = (1 - m_R)/m_f \propto_o \tag{3.21}$$

Note that an iteration process is carried out until a desired accuracy is met $|\propto_a{}' - \propto_a| < 10^{-5}$.

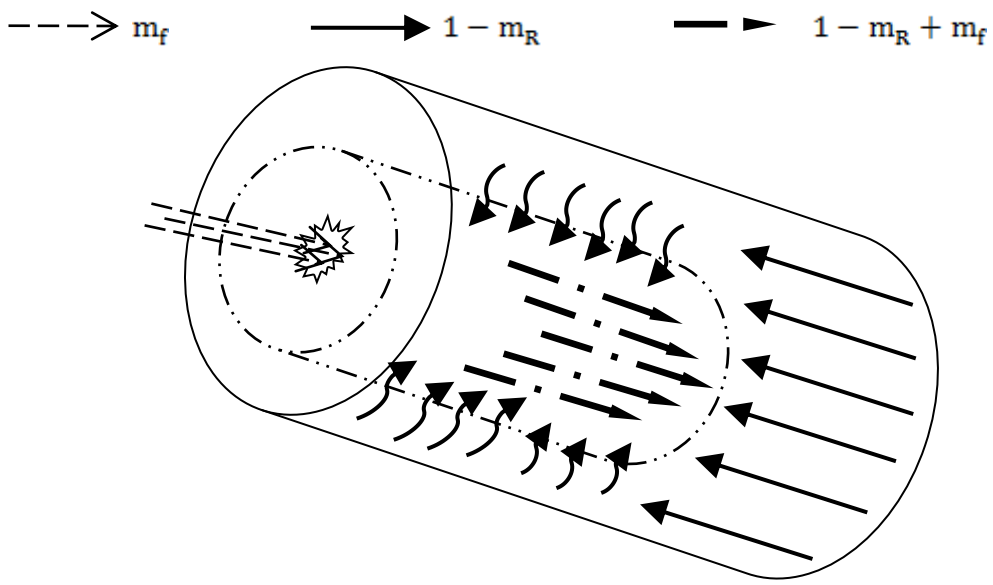

Figure 3.4: Mass balance of a can annular combustion chamber.

The turbine section

The product's gases from the combustion process are expanded in the gas turbine. The cooling air is driven to cool the turbine blades and then expanded in the turbine where it is mixed with the product's gases. So the cooling air is expanded in the gas turbine with a different expansion ratio. The total turbine work is the total of work done by the gases' expansion and air expansion. The excess air coefficient is increased at the exit of the turbine as a result of mixing the cooling air with the exhaust gases.

The gases are expanded from the turbine inlet pressure to the ambient air pressure. Some hydraulic losses are taken into consideration due to the heat recovery steam generator HRSG.

$$P_4 = P_a + dP_4 \tag{3.22}$$

Where P_4 is the pressure at the gas turbine exit and dP_4 is hydraulic resistance after the gas turbine exit, its typical values from 0.02 to 0.03 if the turbine is connected to HRSG. (Alrobaei, 1998)

The gases expansion ratio is equal to:

$$\sigma_T = \frac{P_3}{P_4} \quad (3.23)$$

The following relation allows determining the exhaust gas temperature for isentropic process.

$$T_{4s} = T_3(\sigma_T)^{(1-\gamma_T)/\gamma_T} \quad (3.24)$$

With γ_T is obtained similar to the compression process.

$$\gamma_T{}' = 1/[1 - \left(\frac{r_T}{Cp_T}\right)] \quad (3.25)$$

Note that the specific heat at constant pressure and the gas constant of the exhaust gases are calculated as:

$$Cp = \sum_{i=1}^{4} C_i\, Cp_i \quad (3.26)$$

$$r_T = \sum_{i=1}^{4} C_i\, r_i \quad (3.27)$$

With:

$$Cp_i = a_i + b_i T + c_i T^2 + d_i T^3 \quad (3.28)$$

The following table provides the exhaust gases compositions and theirs parameters.

Table 3.1: Exhaust gases compositions.

Exhaust gas	Mass fraction (Ci)	M [kg/kmol]	r [kJ/kg.K]	a	b ($/10^{-2}$)	c($/10^{-5}$)	d ($/10^{-9}$)
O_2	13.16	31.999	0.2598	25.48	1.520	-0.7155	1.312
N_2	74.514	28.013	0.2968	28.90	-01571	0.8081	-2.873
H_2O	7.893	18.15	0.4615	32.24	0.1923	1.055	-0.3593
CO_2	3.537	44.010	0.1889	22.26	5.981	-3.501	7.469
Others	0.896	-	-	-	-	-	-

The turbine isentropic efficiency can be given by:

$$\eta_{is}^{T} = \frac{(\sigma_T)^{-\left(\frac{\gamma_T - 1}{\gamma_T}\right)\eta_p^T} - 1}{(\sigma_T)^{\frac{\gamma_T - 1}{\gamma_T}}} \quad (3.29)$$

Where η_p^T is the turbine polytropic efficiency, its typical value 0.84 to 0.9.

The enthalpy of the exhaust gas is equal:

$$h_4 = h_3 + \eta_{is}^{T}(h_3 - h_{4s}) \quad (3.30)$$

The relative turbine work for product gases, without taking into account the air cooling system, is equal to (Alrobaei, 1998):

$$W_{SR} = (1 - m_R + m_f)(h_3 - h_4) \quad (3.31)$$

The relative work of the expansion process for product gases in the gas turbine taking into account the effect of cooling air system is:

$$w_{AR} = w_{SR} - \Phi Q_R \quad (3.32)$$

The relative quantity of extraction heat in the cooling system is:

$$Q_R = m_R.(h_R - h_2) \quad (3.33)$$

$$\Phi = 1 - (T_4/T_3) \quad (3.34)$$

The air cooling temperature at the end of the cooling process is given by:

$$T_R = T_2 + (T_b - T_2).\varepsilon_R \quad (3.35)$$

Where ε_R is the cooling system effectiveness. Typical value 0.42 (Alrobaei, 1998)

The expansion ratio for cooling air within the turbine is then evaluated (Alrobaei, 1998):

$$\sigma_R = (1 - \xi_R).\sigma_T \quad (3.36)$$

Where: ξ_R is the expansion coefficient of cooling air. Typical value 0.35 (Alrobaei, 1998)

Then the cooling air temperature at the end of the expansion process T_{4R}.

$$T_{4sR} = T_R(\sigma_R)^{1-\gamma_T/\gamma_T} \quad (3.37)$$

So that:

$$h_{4R} = h_R + \eta_{is}^T(h_R - h_{4sR}) \quad (3.38)$$

The relative work of the cooling air expansion in the gas turbine is calculated (Alrobaei, 1998):

$$W_R = m_R.(h_R - h_{4R}) \quad (3.39)$$

Where: h_R and h_{4R} are, respectively, the enthalpies of cooling air before and after the expansion process.

Total relative work of the gas turbine:

$$W_T = W_R + W_{AR} \quad (3.40)$$

The compressor specific work is given by:

$$W_k = m_k C_{pk}(T_2 - T_1) \quad (3.41)$$

The net gas turbine specific work is equal to the difference between the turbine specific work and compressor specific work:

$$W_{GT} = W_T - W_K \quad (3.42)$$

For a given capacity of a gas turbine the required air mass flow is estimated:

$$m_k = \frac{W_{GT}^{net}}{W_{GT}\,\eta_m\,\eta_e} \quad (3.43)$$

The gas turbine fuel consumption is calculated:

$$M_f = m_f m_k \quad (3.44)$$

The specific fuel consumption of the gas turbine unit:

$$sfc = \frac{M_f}{W_{GT}^{net}} \quad (3.45)$$

The gas turbine unit efficiency is equal to the net output divided by the energy input to the thermal cycle.

$$\eta_{GT} = \frac{W_{GT}^{net}}{M_f Q_{cv}} \tag{3.46}$$

Exhaust gas characteristics:

The mass flow rate of exhaust gases from the gas turbine unit:

$$m_{gas} = m_k(1 + m_f) \tag{3.47}$$

As the cooling air is mixed with the produced gases from the combustion chamber within the expansion process, the final exhaust gases' parameters must be evaluated (Alrobaei, 1998):

$$Q_{gas} = \frac{(1-m_R+m_f).h_4 + m_R.h_{4R}}{(1+m_f)} \tag{3.48}$$

The excess air coefficient is given by:

$$\propto_g = 1/m_f \propto_o \tag{3.49}$$

3.3 The heat exchangers network mathematical analysis

The selected ISCCS consists of a conventional combined cycle power plant, a solar field, and a heat solar steam generator. During sunny periods, one part of feed water is withdrawn from the heat recovery steam generator HRSG converted to saturated steam in the solar steam generator HSSG. This saturated steam is returned to the HRSG where it is mixed and superheated. The increased solar thermal energy provides an increase in the steam mass flow of the Rankine cycle. During cloudy periods and at night, the integrated plant operates as a conventional combined cycle.

As shown in figure 3.5, the heat recovery steam generator is made up of three heat exchangers (An Economizer, a Steam generator and a Superheater). In order to recover some heat from the solar filed, a solar steam generator HSSG is used. During the day, one part of the feed water is withdrawn from the economizer to the HSSG.

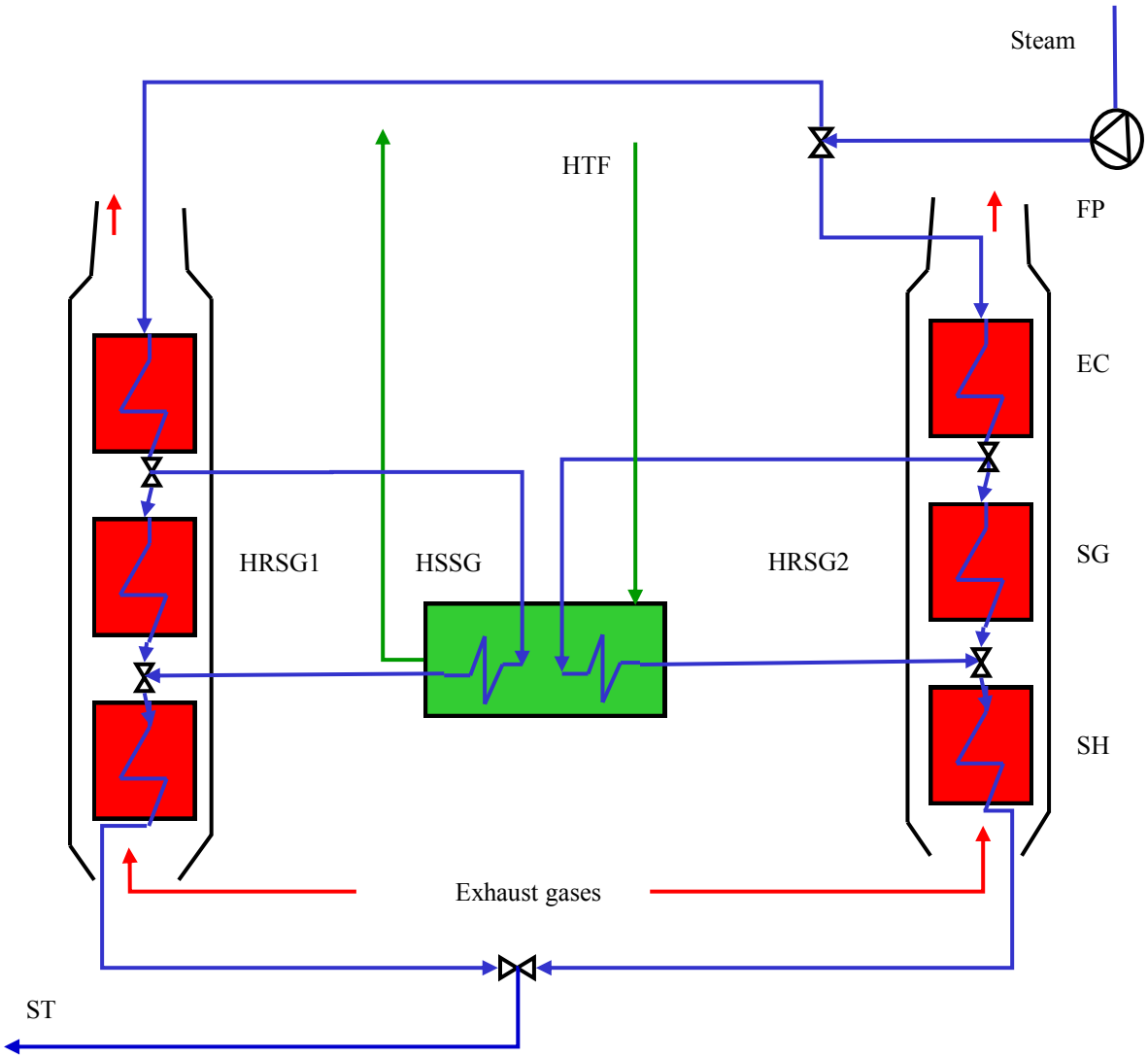

Figure 3.5: Heat exchangers network.

The main purpose of analysing the heat exchangers net work is to determine the input and the output parameters of each exchanger. Estimating steam turbine inlet temperature, the heat solar steam generator mass flow and its temperature is the most important parameters of this analysis.

The first section of the heat exchangers network analysis is the economiser (EC). The water leaves this section as a saturated steam. The water enters the economizer after increasing its pressure by a feed water pump. The feed water pump pressurises the feed water pressure from the deaerator pressure to HRSG pressure. It is assumed that the water feed pump outlet pressure is equal to $P_{FP} = 93$ bars. To simplify, the pressure losses at the heat exchangers networks are omitted.

The inlet steam temperature of the economizer is assumed to be constant (equals to T_{Ve1} =20 °C) and the HRSG exhaust gases outlet temperature is set constant (T_{gs1}= 100°C). By using the energy balance of the economiser the outlet temperature is obtained.

$$T_{Vs1} = \left[\frac{m_g Cp_{g1}(T_{ge1} - T_{gs1})}{\mathrm{m_{ST}}\, Cp_{V1}}\right] + T_{Ve1} \tag{3.50}$$

Where: $Cp_{g1}$and $Cp_{V1}$are, respectively, the average specific heat of the exhaust gases and the steam in the economiser.

From a thermodynamic point of view, the solar heat input should be used for the replacement of latent heat and at the highest possible temperature level (J. Dersch et al). The temperature of the heat transfer fluid HTF is limited to 393°C to avoid decomposition; therefore, maximum solar steam temperatures of about $T_{so} = 372$ °C are chosen. From sunrise to sunset the steam leaves the economizer divided into two parts. One part exceeds the steam generator (SG) of the HRSG and the other part passes through the HSSG. Their quantities are depending on the initial steam parameters and the solar energy which is supplied to the HSSG. The mass flow which passes through this latter is calculated based on the solar field output.

$$m_{Vs} = Q_{SF}/(H_{ss} - H_{s2}) \tag{3.51}$$

At the steam generator, the steam outlet temperature is calculated based on the exhaust gases' parameters and the mass flow of this steam. The steam mass flow is deduced from the mass conservation.

$$m_{V2} = m_{ST} - m_{Vs} \tag{3.52}$$

$$T_{Vs2} = \left[\frac{m_g Cp_{g2}(T_{ge2} - T_{gs2})}{\mathrm{m_{V2}} Cp_{V2}}\right] + T_{Ve2} \tag{3.53}$$

Where: $Cp_{g2}$and $Cp_{s2}$are, respectively, the average specific heat of the exhaust gases and the steam at the SG.

The first value of the steam turbine mass flow m_{ST} is assumed, then the solutions for equations (3.50) to (3.53) are determined, after which an iteration process is carried out until a desired

accuracy is met $|T_{Vs2} - T_{so}|$<0.001. Consequently the actual conditions at the superheater inlet are achieved.

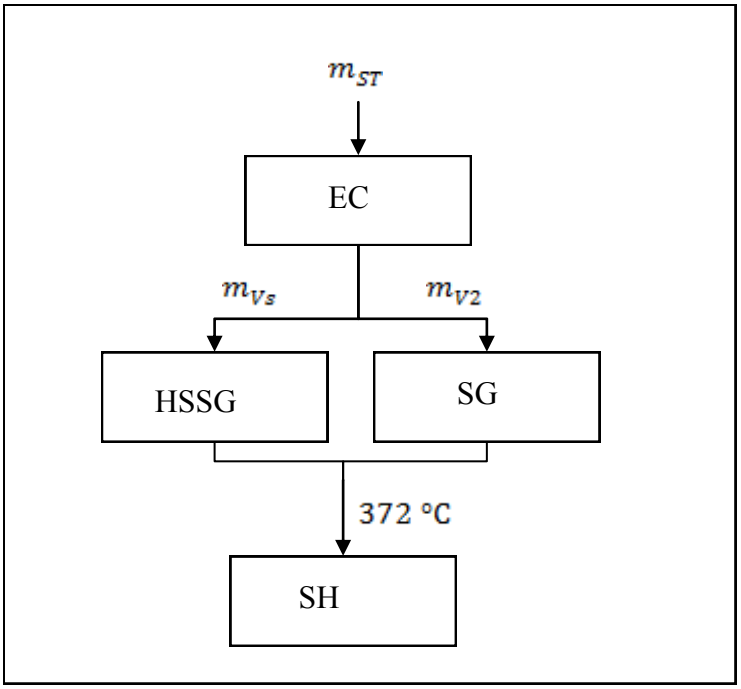

Figure 3.6: Mass flow through the heat exchangers network.

At this level, the exhaust gas temperature is given assuming that it is above the steam temperature inlet by the minimum allowed temperature difference.

$$T_{gs3} = T_{Vs2} + \Delta T \tag{3.54}$$

The last section of HRSG analysis is the superheater (SH). The steam leaves the HSSG as a saturated steam or slightly superheated enters this section after it is mixed with the SG steam flow. The SH steam inlet temperature remains constant by the variation of the steam turbine mass flow. The steam turbine inlet temperature is calculated from the energy balance of the superheater.

$$T_{Vs3} = \left[\frac{m_g Cp_{g3}(T_{ge3} - T_{gs3})}{\mathrm{m_{ST}}\, Cp_{V3}}\right] + T_{Vs2} \tag{3.55}$$

Where: $Cp_{g3}$and $Cp_{V3}$are, respectively, the average specific heat of the exhaust gases and the steam in the exchanger SH.

3.4 The steam turbine output

Steam enters the turbine at a high temperature and high pressure superheated state from the superheater. The expansion of the steam as it moves from high pressure to lower pressure converts the potential energy to kinetic energy by imparting its momentum to the turbine blades, thereby causing the shaft to rotate. The mechanical work created by the rotating shaft is converted to electrical energy by a generator. The electricity generating can be given as:

$$W_{ST}^{net} = W_{ST} - W_{FP} \tag{3.56}$$

3.5 Integrated solar combined cycle performances

The most important factors to evaluate the ISCCS are the net output and the efficiency. The net output of the plant is best determined by calculating the instantaneous output of the gas turbines and steam turbine, and summing the results.

$$W_{ISCCS} = 2\, W_{GT}^{net} + W_{ST} \tag{3.57}$$

The efficiency is then can be calculated:

$$\eta_{ISCCS} = \frac{W_{ISCCS}}{M_f Q_{cv}} \tag{3.58}$$

The net solar output is the difference of the steam turbine output between sunny and night periods.

$$W_{ss} = {W_{ST}}^{ISCCS} - {W_{ST}}^{CC} \tag{3.59}$$

The solar electricity ratio is:

$$R_{so} = \frac{W_{ss}}{W_{ISCCS}} \tag{3.60}$$

4. SIMULATION AND RESULTS

4.1 The gas turbine subprogram

By using the thermodynamic analysis which is represented in section 3.2, the gas turbine model is achieved. This latter is applied to evaluate the gas turbine performances and the exhaust gases conditions as a function of the ambient temperature.

The gas turbine subprogram, which is represented in figure 4.1, uses the data shown in table 4.1 and starts by calculating the pressures through the gas turbine. This allows obtaining the pressure at the first stage of the compressor. A guessed value for specific heat ratio γ_k for air assumes to obtain the end conditions of the compression process. A correlation for specific heat at constant pressure is utilized to find a new value of γ_k. Then an iteration process is used to calculate the temperature and the specific heat at the compressor outlet.

After that, an experimental correlation is used to estimate the mass flow rate of the cooling system. Then, the fuel mass flow rate is obtained by utilizing the energy balance of the combustion chamber. It is assumed that the inlet turbine temperature is set invariable.

Similarly to the compressor section, the final parameters of the expansion process are finding. By analyzing the cooling system the output of the turbine is determined. Then, the gas turbine efficiency, the exhaust gases masses and its temperature are obtained.

Note that all the previous parameters are obtained at standard conditions. Then, an iteration to display the gas turbine performances as function of the ambient temperature is used.

The purpose of evaluating the gas turbine is to quantify the exhaust gas heat which will be utilized in the heat recovery steam generator. That's why, the exhaust gases parameters are exported to the principal program.

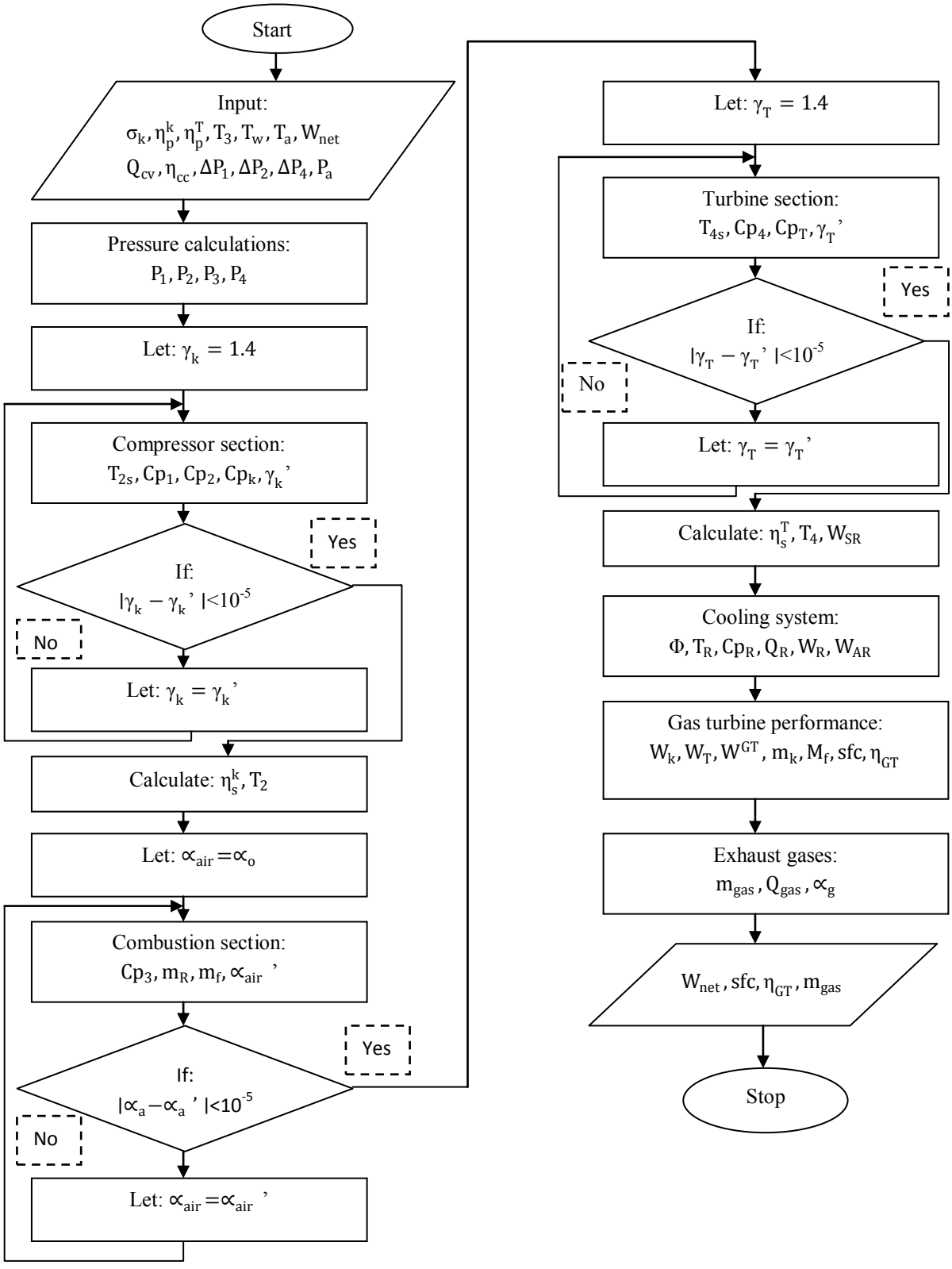

Figure 4.1: The gas turbine flow chart.

Table 4.1: Data to the gas turbine subprogram.

Parameters	Symbols	values	Units
Ambient temperature	T_a	15	°C
Turbine inlet temperature	T_3	1200	°C
Turbine blade temperature	T_b	850	°C
Cooling system effectiveness	ε_R	42	%
Expansion coefficient of cooling air	ξ_R	35	%
Turbine polytropic efficiency	η_p^k	90	%
Compressor polytropic efficiency	η_p^T	91	%
Combustion efficiency	η_{cc}	98	%
Mechanical efficiency	η_m	98	%
Electrical efficiency	η_e	98.5	%
Atmospheric pressure	P_a	1.013	bar
Compressor inlet pressure losses	dP_1	0.005	Bar
HRSG pressure losses	dP_4	0.025	Bar
Combustion pressure losses	dP_2	0.020	Bar
Natural gas calorific value	Q_{cv}	45.806	MJ/kg
Gas turbine output (standard conditions)	W_{net}^{GT}	47	MW
Air to fuel ratio	$\propto_o$	15	---
Compression ratio	σ_k	19.9	---

Table 4.2: Results of the gas turbine subprogram (standard conditions)

Parameters	Symbols	values	Units
Compressor section			
outlet temperature	T_2	451	°C
Average specific heat ratio	γ_k	1.38	---
Isentropic efficiency	η_s^k	85.37	%
Average Specific heat Cp	Cp_k	1.03	kJ/kg.K
Specific Work consumption	W_k	450.60	kJ/kg
Turbine section			
Average Specific heat Cp	Cp_T	1.27	kJ/kg.K
Isentropic efficiency	η_s^T	87.90	%
Average specific heat ratio	γ_T	1.30	---
Specific work	W_T	826.19	kJ/kg
Cooling system			
Mass flow rate	m_R	3.12	%
Cooling air outlet temperature	T_R	631	°C
Cooling air work in the turbine	W_R	11.43	kJ/kg
Gas turbine unit performances			
Net specific work	W_{GT}	375.58	kJ/Kg
Gas turbine efficiency	η_{GT}	38.5	%
Compressor air mass flow	m_k	129	kg/s
Exhaust gases temperature	T_4	551	°C
Excess air coefficient of the exhaust gases	$\propto_g$	3.2	---
Gas turbine fuel consumption	M_f	9579	kg/h
Specific fuel consumption	sfc	9.34	MJ/kW.h
Exhaust gas energy	Q_{gas}	123.04	MW

4.2 The gas turbine subprogram validation

Gas turbines, which are selected for the ISCCS of Hassi R'mel, are from Siemens Corporation. It is named SGT 800. In order to check the performance of the gas turbine subprogram, its results will be compared with the design data of the SGT800.

The compressor air mass flow, the exhaust mass flow and its temperature, the specific fuel consumption and the gas turbine efficiency are the most important parameters to check the performances of this gas turbine subprogram.

Standard conditions are preferred for this type of comparisons.

Table 4.3 Subprogram validation

The most important parameters		SGT 800	Gas turbine (GT) subprogram	Error (%)
compressor air flow	(kg/s)	129	129	0.0
Exhaust gases mass flow	(kg/s)	131,5	131	0.3
Exhaust gases temperature	(°C)	544	551	1.2
Specific fuel consumption	(MJ/kW.h)	9.6	9.36	2.5
Gas turbine efficiency	(%)	37.5	38.5	2.6

As shown in the table above the gas turbine subprogram results are very accurate. For instance, an exact value of the compressor airflow is achieved. Consequently, it can be used to simulate the performances of integrated plant.

4.3. Solar field subprogram

The flow chart of the subprogram which is represented in figure 4.2 is used to simulate the solar field of ISCCS based on the Hassi R'mel climate conditions. The average ambient temperature is assumed to be constant and equals 30°C.

The program calculates instantaneous heat and mass balances on the solar field. The thermal input from the solar field is estimated by calculating the following:

• Solar time, sunrise and sunset times.

• Each of the following angles: solar declination, sun elevation, sun azimuth, and collector incidence.

•From the collector incidence angle, an incidence angle modifier is calculated to account the reflected radiations which miss the end of the heat collection element.

•The instantaneous direct normal irradiation is then estimated from sunrise to sunset using the HOTTEL method.

• The absorber temperature and the heat losses coefficients.

• After employing the energy balance between the incoming solar radiations and heat losses, parabolic trough concentrator output is obtained.

• Net solar field thermal output, by multiplying the solar collector output, the number of collectors and the energy transportation efficiency of the field piping.

The design point in which the solar thermal output is the highest is obtained by using iteration as a function of the time of year. Finally, the solar thermal output is exported to the principal program.

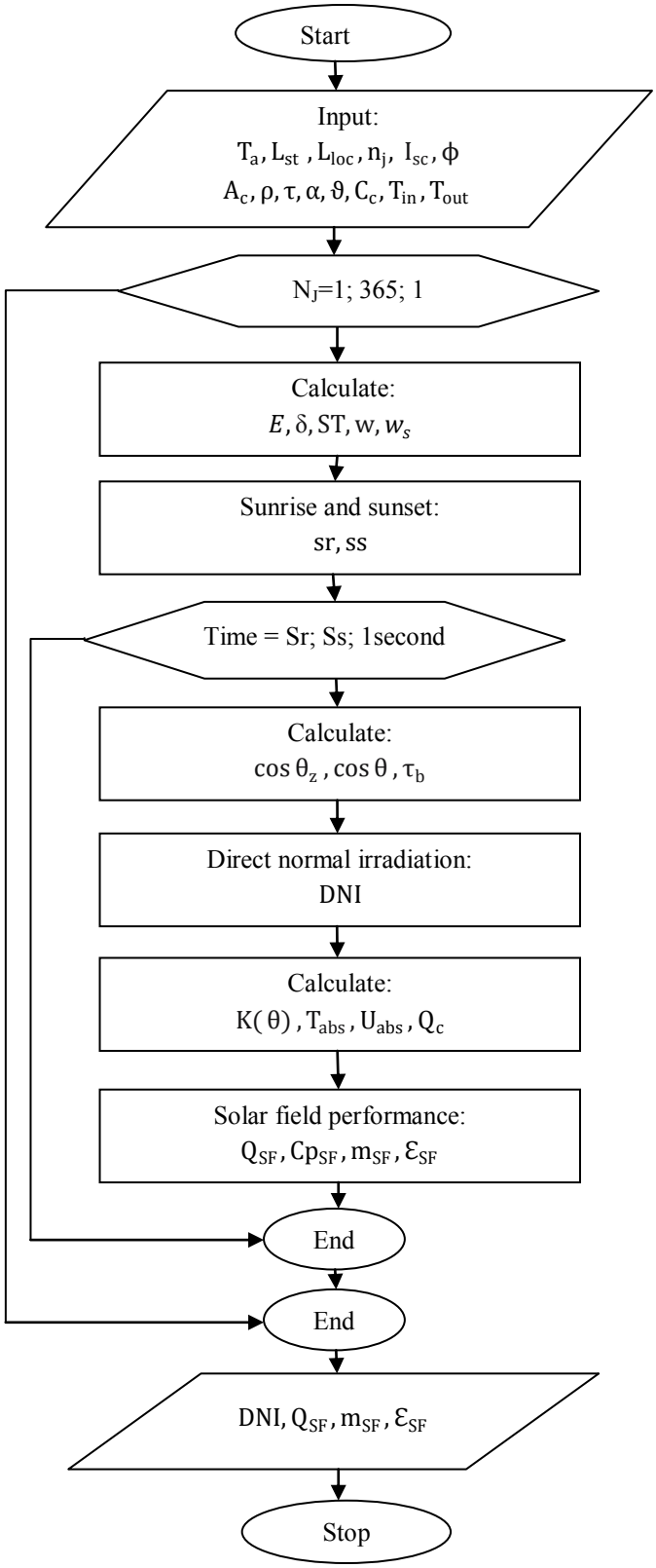

Figure 4.2: Solar field flow chart.

Table 4.4: Data to the solar field subprogram

Parameters	Symbols	values	Units
Solar constant	I_{sc}	1367	W/m^2
Ambient temperature	T_a	30	°C
Solar field			
HTF inlet temperature	T_{in}	290	°C
HTF outlet temperature	T_{out}	393	°C
Number of collectors in each row	C_L	4	---
Number of lines	N_L	56	---
Solar collector area	A_c	817.5	m^2
Energy transportation efficiency	η_{tr}	98	%
Collector optical performances			
intercept factor	ϑ	96	%
Absorptivity	α	95	%
Reflectivity	ρ	98	%
Transmissivity	τ	97	%
Concentration ratio	C_c	82	---
Hassi R'mel location			
Altitude	α_s	776	m
Longitude			
Latitude	Φ	33.8	Degree
Climate type	---	Tropical	---

4.4. The solar field subprogram results

In order to evaluate the instantaneous performances of the solar field, it is necessary to estimate the solar radiation intensity from sunrise to sunset. The direct normal irradiation, of course, depends on the local weather conditions at the site where the power plant is built.

Figure 4.3 illustrates the instantaneous variation of the direct solar irradiation during the year. This figure shows that the DNI is higher at midday for each day and reaches its highest point in summer. Its value can be expected to reach 900W/m^2 at the design point.

In the operation strategy, the inlet and outlet temperatures of the heat transfer fluid (HTF) remained constant and equal 290, 393 °C respectively. Figure 4.4, 4.5 and 4.6 represent the instantaneous HTF mass flow, the thermal efficiency and the output of the solar field during the year. They all increase according to the rise in the direct solar irradiation from sunrise till sunset of each day, where the operation duration varies for each day.

The period of peak solar field output generally occurs between 10 am to 16 pm from March through September. In summer, the solar thermal energy is about 130 MWth at midday. At this time, the HTF mass flow is in the order of 532 Kg/s. As a result, the solar field efficiency reaches 0.81.

The following figures (4.7, 4.8, 4.9 and 4.10) show the solar field performances for the representative days of four different months. These months are chosen to illustrate the solar field performances at different seasons of the year. The selected days are 21th March, 21th June, 21th September and the 21th December.

The HTF mass flow rate, the thermal efficiency and solar field output increase according to the rise in solar radiation from sunrise till sunset of each day, where the operation duration varies for each day. The amount of solar field output during the summer is greater than for the other seasons due to the higher solar radiation intensity and longer solar radiation duration.

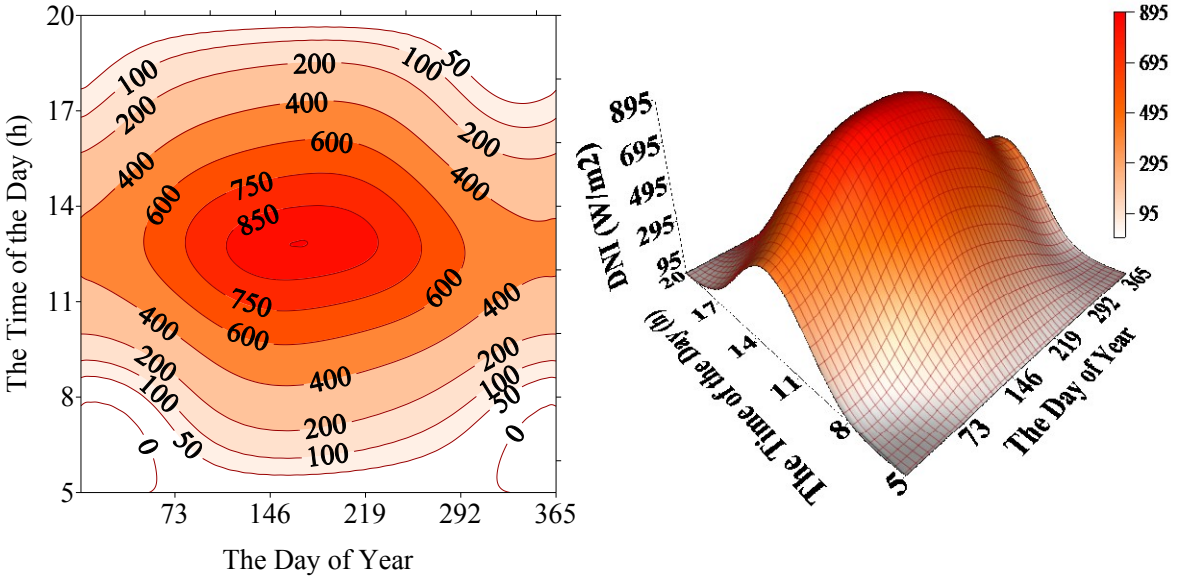

Figure 4.3: The instantaneous direct solar ardiation DNI during the year (W/m^2).

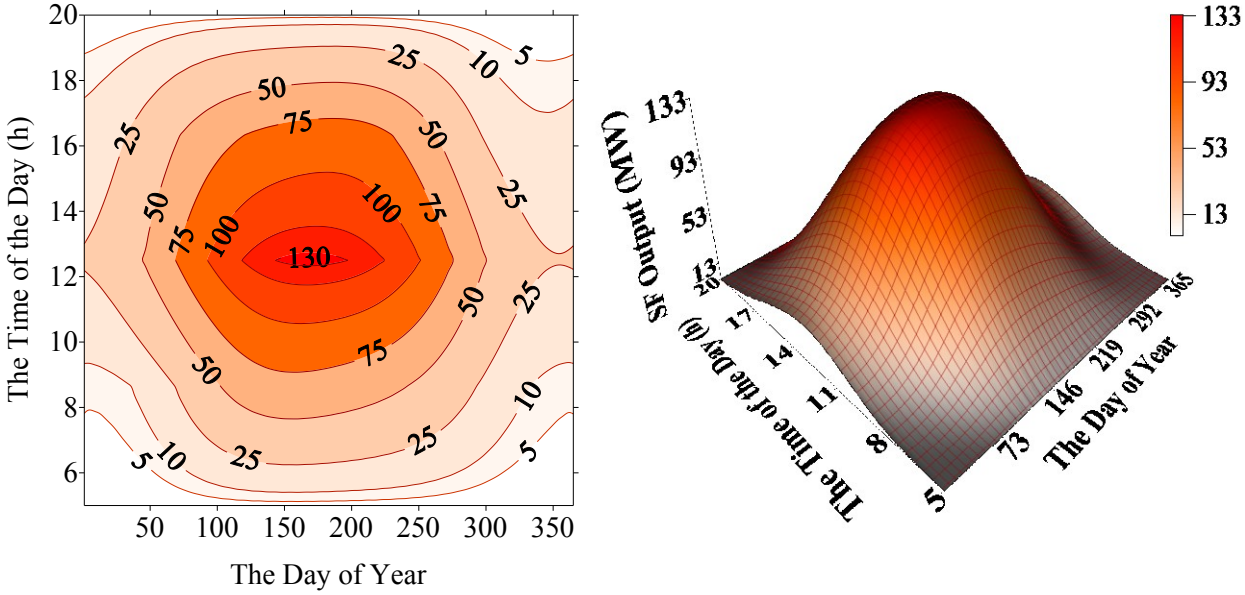

Figure 4.4: The instantaneous solar field output (MW) during the year.

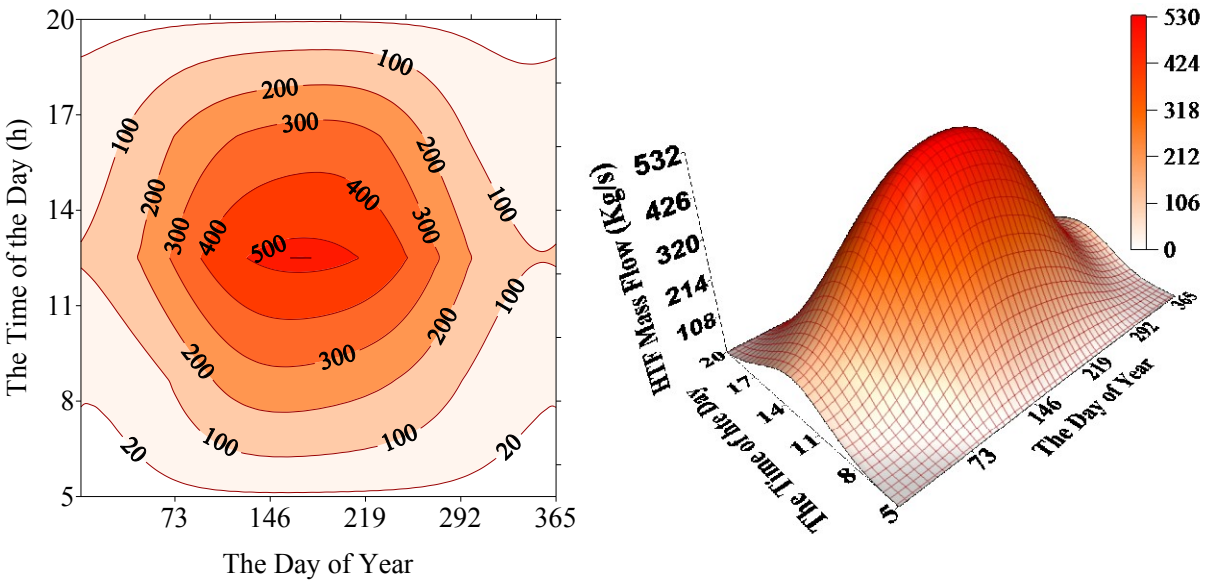

Figure 4.5: The Variation of HTF mass flow during the year (kg/s) .

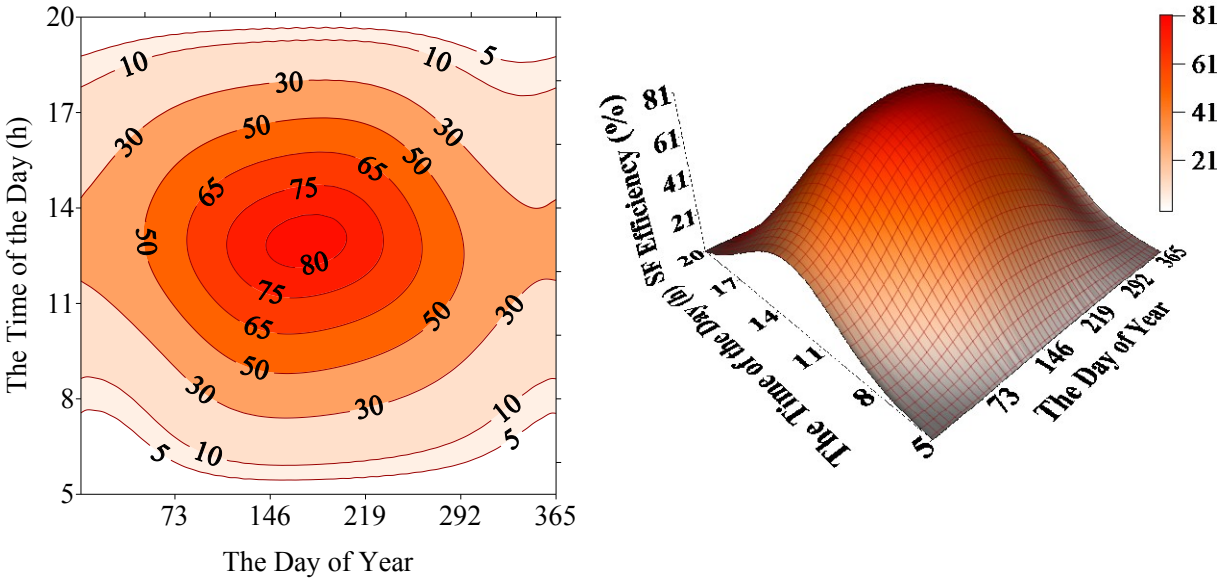

Figure 4.6: The instantaneous solar field efficiency (%) during the year.

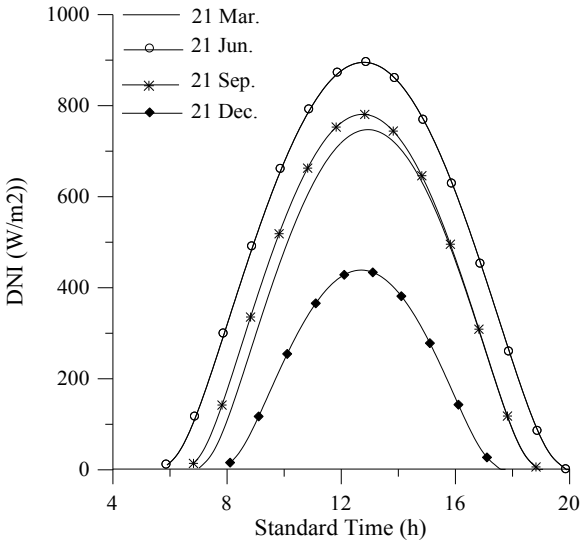

Figure 4.7: Direct Normal Irradiation (W/m^2) at the four selected days.

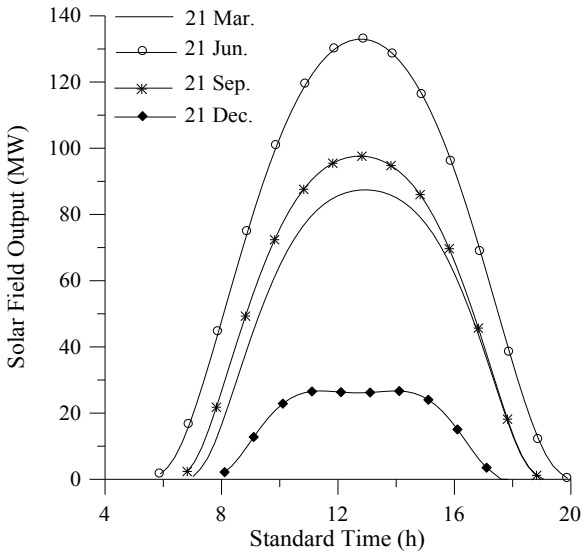

Figure 4.8: Solar Field Output (MW) at the four selected days.

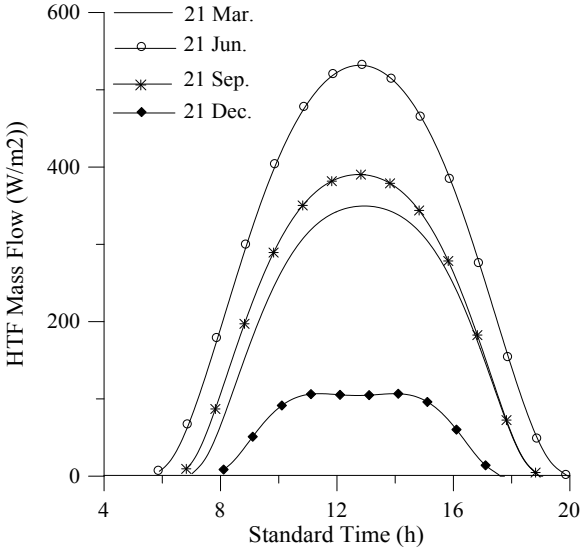

Figure 4.9: HTF Mass Flow (Kg/s) at the four selected days.

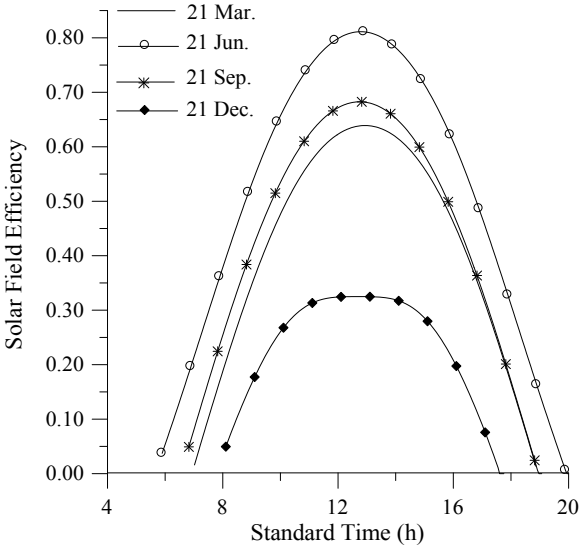

Figure 4.10: Solar Field Efficiency at the four selected days.

4.5. The ISCCS program

The flowchart of the principal program which is employed to predict the ISCCS performance is outlined in figure 4.11. This program is based on the thermodynamic analysis which is presented in chapter 3. The average ambient temperature is assumed to be constant and equals 30°C.

The program starts by calculating the sunrise and sunset times for each day to simulate the ISCCS during the daytime. At night, the power plants work as a CC. The combined cycle solution is included in this program. The gas turbine subprogram is then run to provide the exhaust gases conditions.

Solving the Economizer of the HRSG is the second step. From sunrise till sunset the power plant is operated as ISCCS. The solar field subprogram is then applied for supplying the solar thermal energy to HSSG. By analyzing this latter, the generated solar steam mass flow rate is obtained. The exported steam to the Steam generator SG of the HRSG is equal to the generated steam in the economizer minus the extracted steam for the HSSG. The proposed design is operated as a combined cycle at night, so the HRSG characteristics for this operation system are calculated.

In the proposed operation strategy, the superheater steam inlet temperature is remained constant by the variation of the steam turbine mass flow. The first value of the steam turbine mass flow is assumed, then the optimum mass is carried out, after which an iteration process is employed until a desired accuracy is met $|T_{Vs2} - T_{so}| < 10^{-3}$. Consequently, the actual conditions at the superheater inlet are achieved. At this level, the exhaust gas temperature is given assuming that it is above the steam temperature inlet by 70°C. After employing the energy balance of the SH, the steam turbine inlet temperature is determined. Then its performances are evaluated.

The output for the CC regime is constant and the output for the ISCCS varies with the solar radiation variation. Finally, an iteration process at the ambient temperature to evaluate the ISCCS performances is employed.

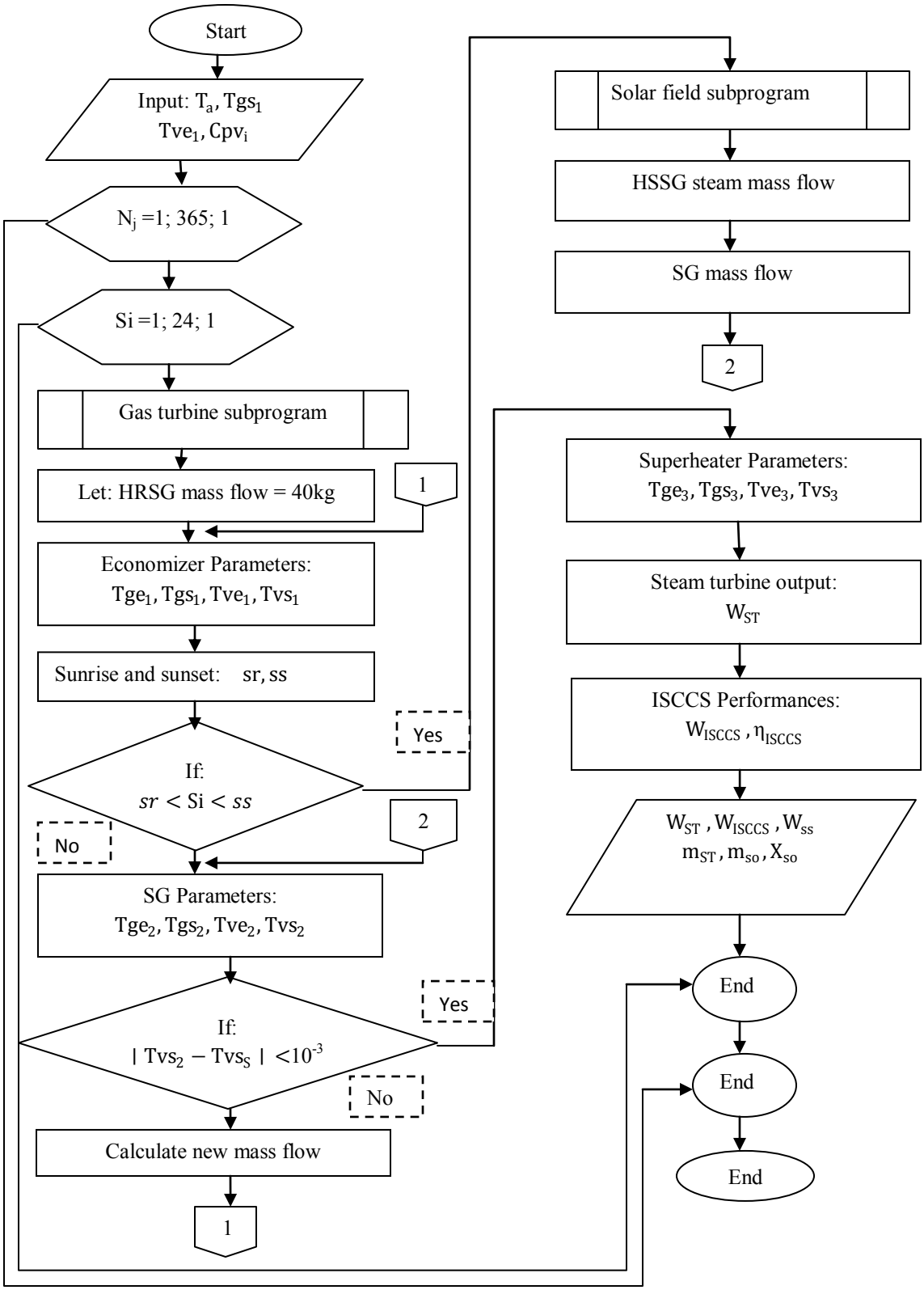

Figure 4.11: ISCCS program flow chart.

Table 4.5: Principal components of the ISCCS

Components	Number
Gas turbine	2
HSSG	1
HRSG	2
Steam turbine	1

Table 4.6: Data to the ISCCS program

Parameters	Symbols	values	Units
Ambient temperature	T_a	30	°C
Atmospheric pressure	P_a	1	bar
HRSG exhaust gas outlet temperature	T_{gs1}	100	°C
HRSG steam inlet temperature	T_{ve1}	20	°C
HSSG steam outlet temperature	T_{ss}	372	°C
The minimum temperature allowed at the SH	ΔT	70	°C
Steam turbine thermal efficiency	η_{ST}	37.5	%
Steam turbine electrical efficiency	η_e	98	%
Steam turbine thermal efficiency	η_m	98	%

4.6. The ISCCS program results

The data to the principal program are presented in table 4.5 and 4.6. The operation parameters of the HRSG are obtained by using the mathematical analysis of chapter 3. The results of the ISCCS program are illustrated in the following seven figures.

From a thermodynamics point of view, for the Rankin cycle, it is desirable to increase the steam mass as solar energy increases. The limit for increasing the temperature of this steam is the exhaust gas temperature. As shown in figures 4.12 and 4.13, the steam mass flow of the HRSG varies according to the HSSG steam mass flow.

This latter is fluctuating as a function of the solar radiation from sunrise to till sunset of each day. As represented in figure 4.13, this quantity can get higher than 30 Kg /s when DNI is higher.

The solar electricity and its fraction vary from sunrise to sunset according to the solar radiation fluctuation. The instantaneous net electrical solar fraction, as shown in figure 4.16, is higher at midday and in summer. The values for this fraction are based on the difference in electrical output of the ISSCS mode and CC mode. As shown in figure 4.14, the total steam turbine output is equal to 69 MW at the design point which means an increase in electricity generation by about 23 MW compared to 46 MW at night.

Figure 4.17 give us an idea about the instantaneous output of the power plant during the year under Hassi R'mel climatic conditions. The ISCCS power plant without solar energy input (at night and during cloudy periods) operates in part load as a combined cycle and produces about 134 MW. As the first solar beam appears, the plant starts to work as ISCCS and the net electricity is augmented according to solar energy. In general, the power plant would like to generate around 150 MW at mid day during the year unless in winter when the increase in electricity is about 5MW only. At design point, the power station will generate around 157 MW, if the sky is very clear.

The ISCCS efficiency is the best factor for evaluating its performances. Looking at figure 4.18 exclusively, it can be observed that the efficiency at night is equals to 57.5%. This confirms the optimization of the combined cycle with one pressure level which is proposed. When ISCCS power plant operates within solar input, the overall net efficiency will be higher than the efficiency at night. The highest value 67% is reached in summer when direct solar irradiation reaches its highest point.

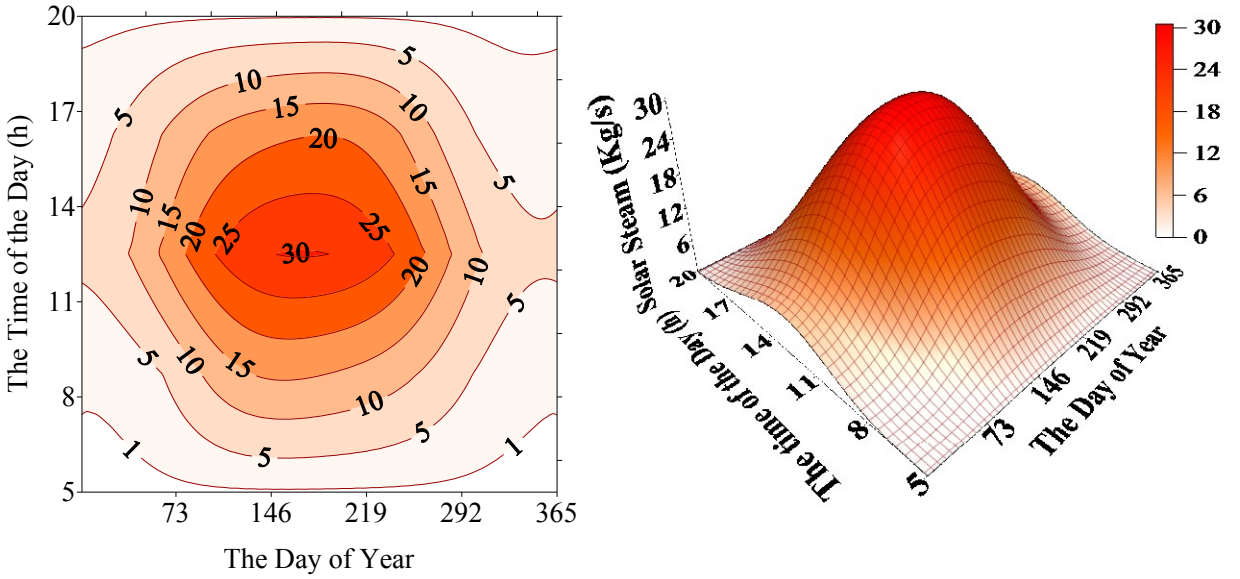

Figure 4.12: The Variation of HSSG steam mass flow during the year (kg/s) .

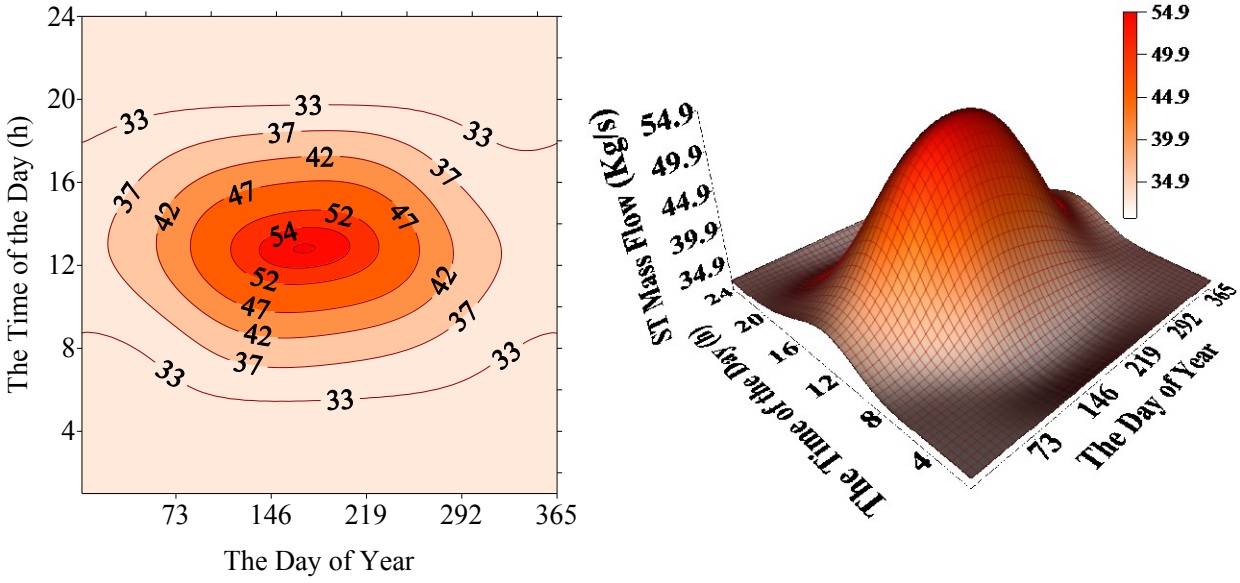

Figure 4.13: The Variation of HRSG steam mass flow during the year (kg/s)

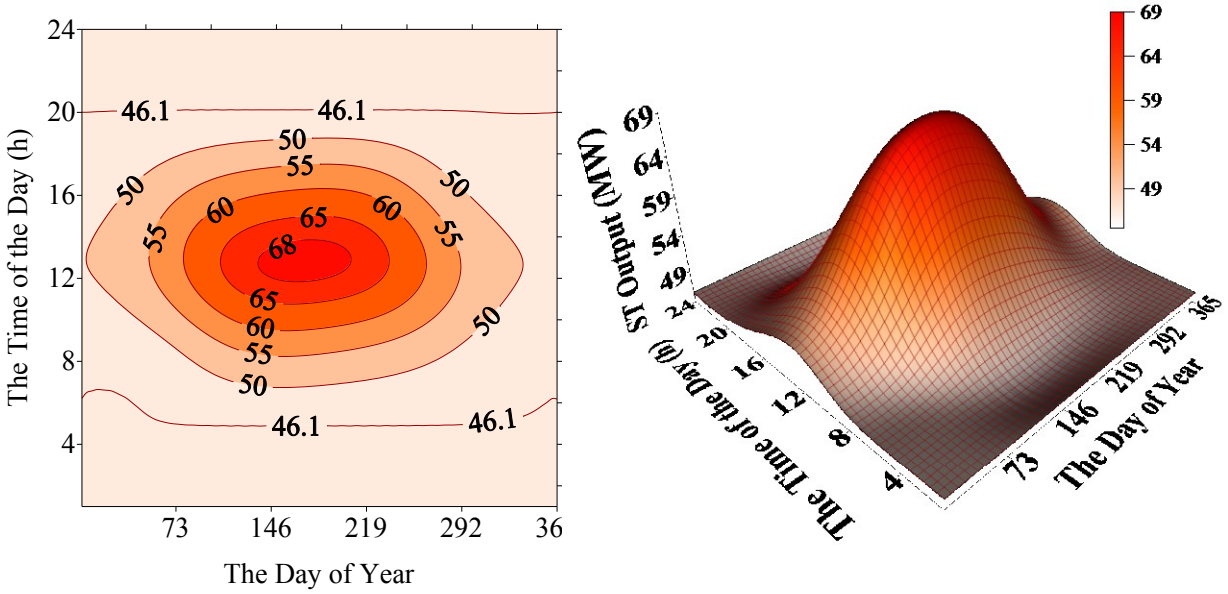

Figure 4.14: The instantaneous Steam Turbine Output (MW) during the year.

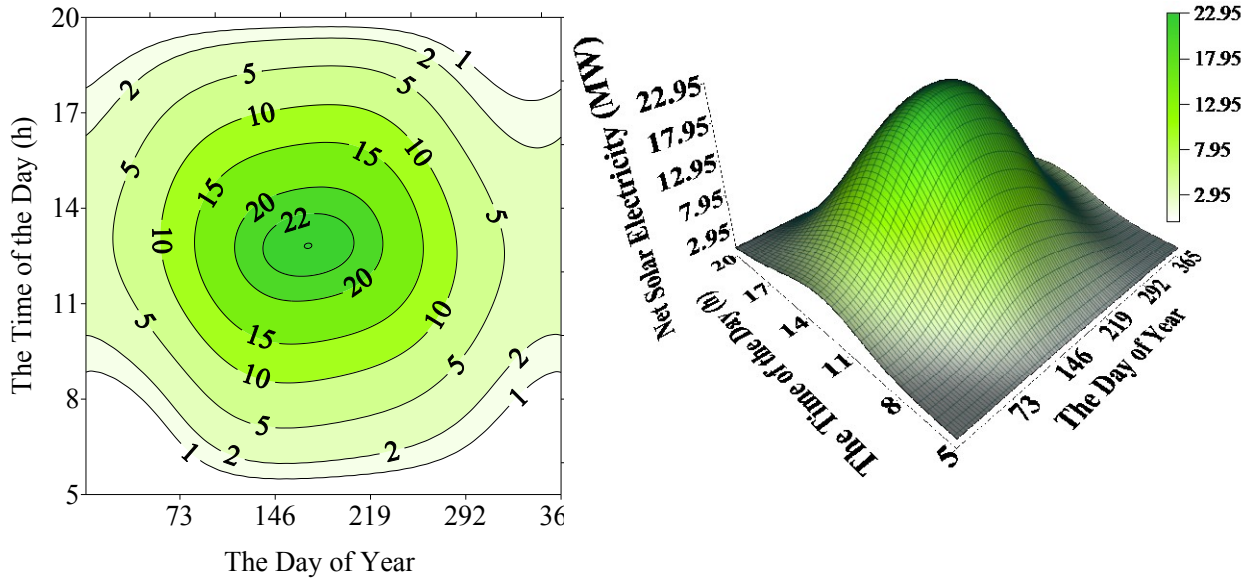

Figure 4.15: The instantaneous Net solar Electricity (MW) during the year.

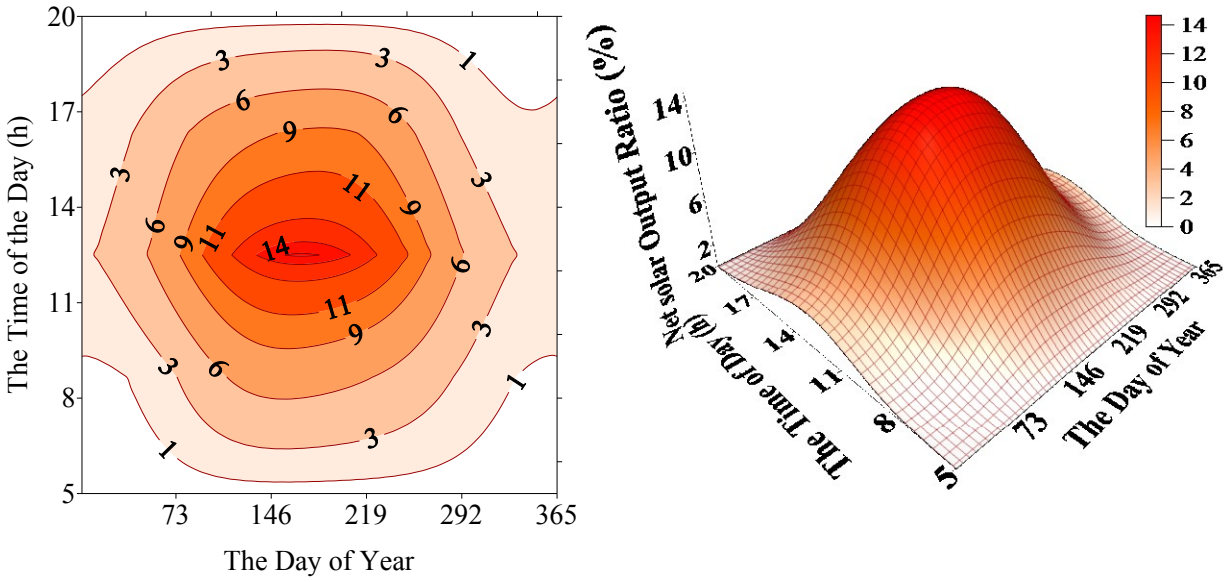

Figure 4.16: The instantaneous Net solar Electricity Ratio (%) during the year.

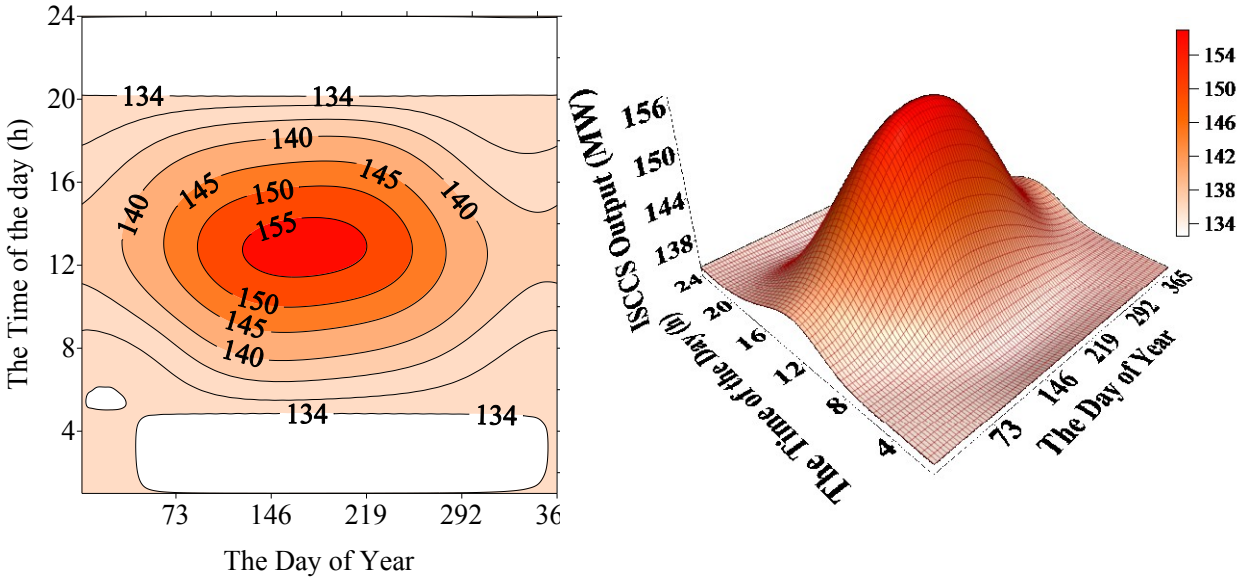

Figure 4.17: The instantaneous ISCCS Output (MW) during the year.

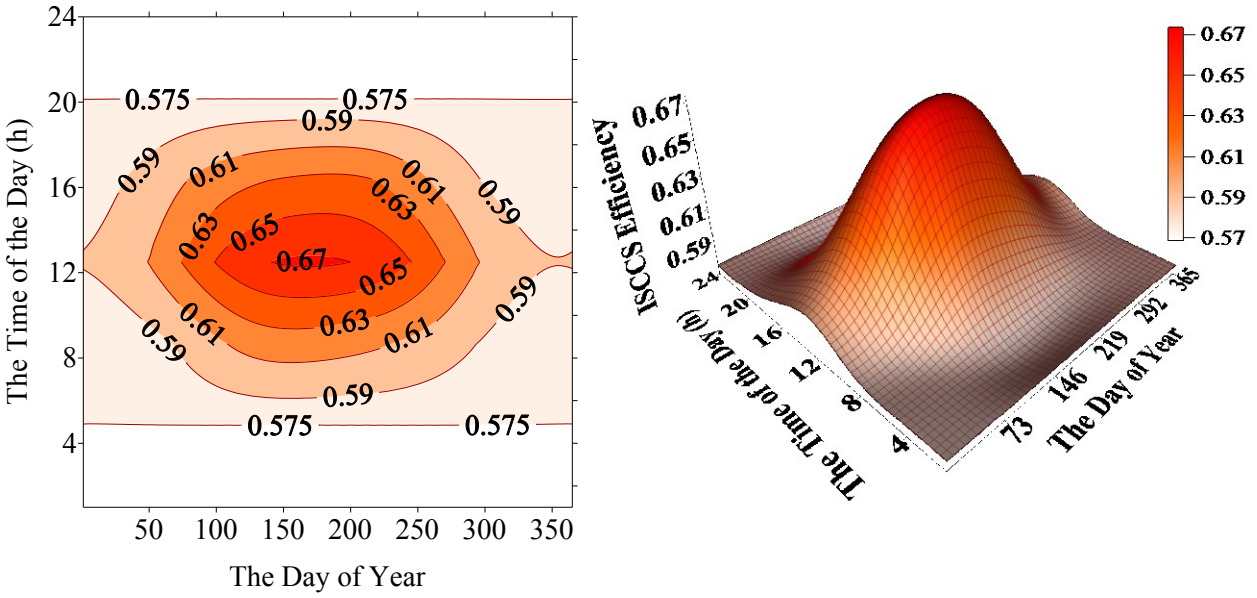

Figure 4.18: The instantaneous ISCCS efficiency during the year.

The following figures illustrate the performances of the integrated plant on representative days of four different months. These days are chosen to illustrate the ISCCS performances at different seasons of the year. The selected days are 21th March, 21th June, 12th September and the 121h December.

Figure 4.19 and 4.20 show the electricity production and the efficiency of the power plant. The output for the CC operation is 134 MW. This amount is the electricity generation at night time. From sunrise to sunset the amount of electricity varies according to the solar radiation intensity variation. As shown in figure 4.19, the total generated energy during summer is greater than for the other seasons due to the higher solar radiation intensity and longer solar radiation duration and the ISCCS output can reach the level of 157 MW. The solar field increase improves the output of the steam turbine where the gas turbine fuel consumption remains constant. As a result of this improvement the output for the ISCCS operation is improved. The net electric output from the solar energy is represented in figure 4.21. Its ratio can reach the limit of 15% at summer when the DNI is in its highest point.

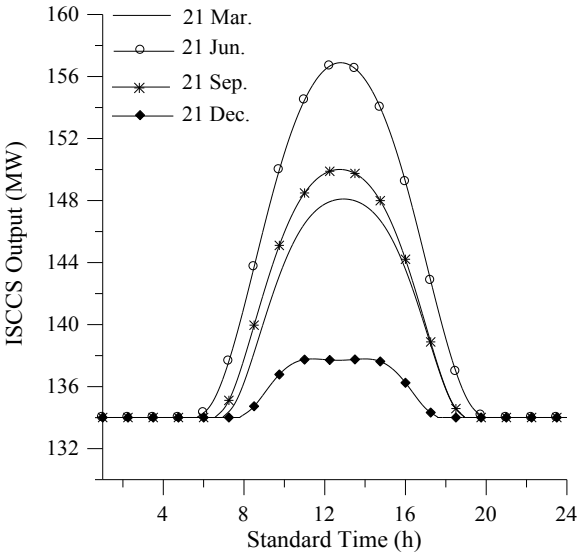

Figure 4.19: ISCCS Output at the four selected days.

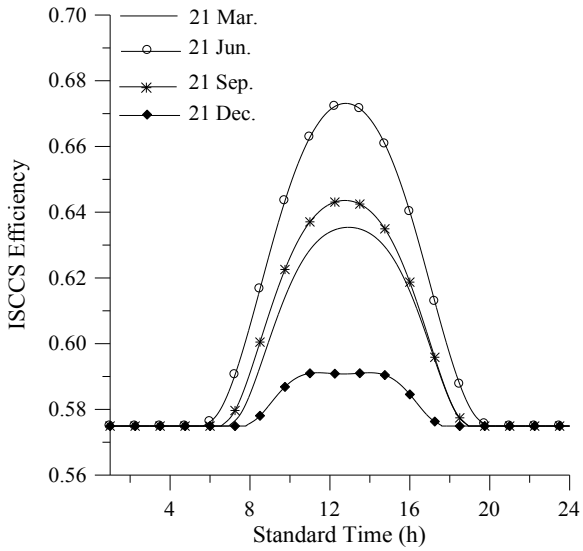

Figure 4.20: ISCCS Efficiency at the four selected days.

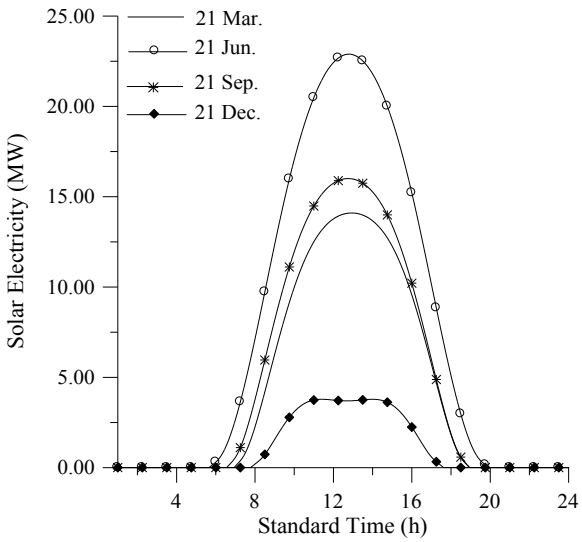

Figure 4.21: Solar Electricity at the four selected days.

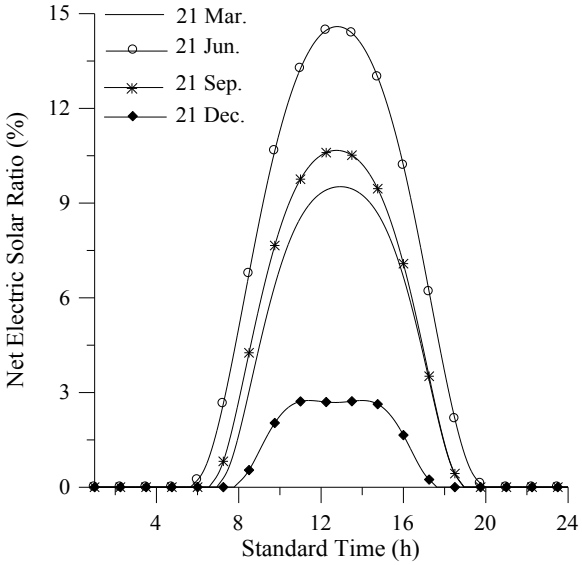

Figure 4.22: Net Solar Electric Ratio at the four selected days.

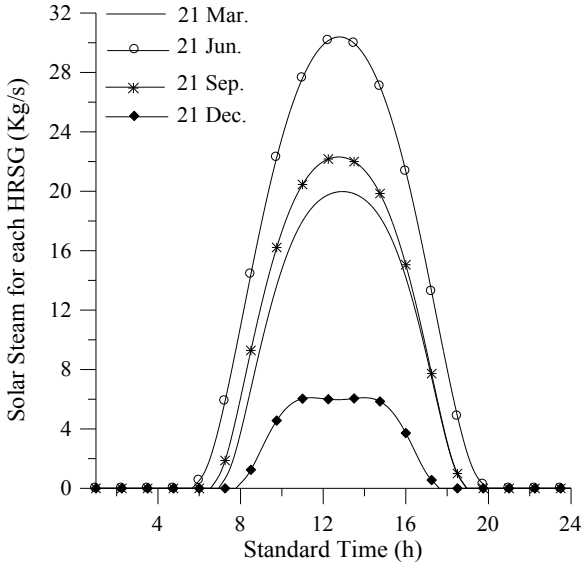

Figure 4.23: Solar Steam (Kg/s) for each HRSG at the four selected days.

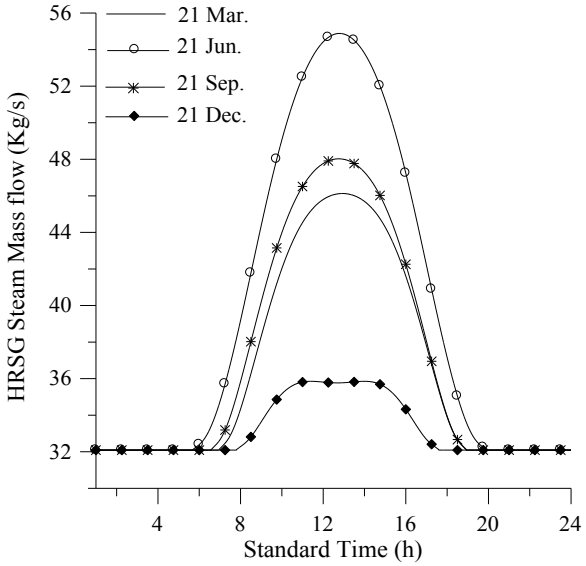

Figure 4.24: HRSG Steam Mass Flow (Kg/s) at the four selected days.

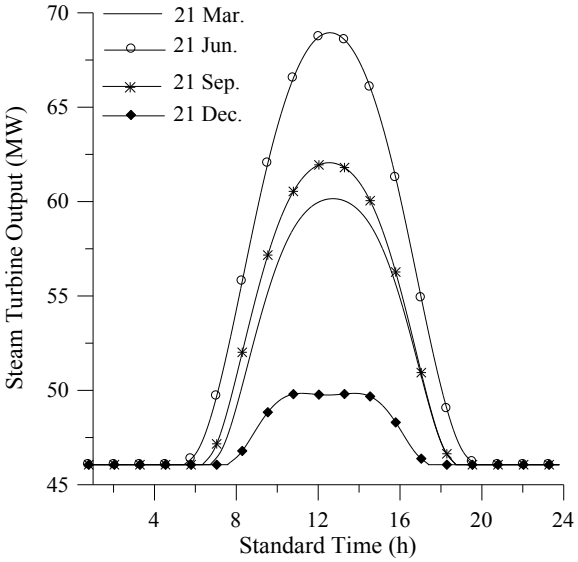

Figure 4.25: Steam Turbine (MW) Output at the four selected days.

4.7. The sensitivity of the ISCCS at ambient temperature

From the solar field subprogram, the day of the year and the time of the day in which the DNI in the highest possible is find out. This time is called the design point. The maximum solar field output is achieved at this point. The design point is obtained on 15 June (the day number 166) with direct solar irradiation go up 895.4 W/m^2.

These data is then exported to the principal program in order to estimate the performances of the power plant as function of the ambient temperature. For this reason, iteration process is made at ambient temperatures. Since this temperature is different than the design point value of 30 °C, each calculation is an off design analysis. Two dimensional curve fits to show the effect of ambient temperature, are developed.

Figure 4.26 and 4.27 illustrate the output from and the efficiency of each part of the power plant as a function of the ambient temperature. The gas turbine output and its efficiency are both decreased sharply with the ambient temperature. An increase of this latter by 5 °C means the waste of 1MW. As a conclusion, the efficiency and the output from the gas turbine are strong functions of the ambient temperature.

Look at the two figures once more slowly. Even though the ISCCS efficiency is increased according to the ambient temperature, its output drops slightly. Another principal exception is the performances of the steam turbine, which was a weak function of the ambient temperature. Thus, the performance of the plant is best determined by calculating the outputs of the steam turbine from sunrise to sunset while the direct normal irradiation varies as a function of the time.

As explained previously, the HRSG mass flow varies according to solar energy fluctuation. In order to provide more explanation for figure 4.26 and 4.27, two iterations are made at ambient temperatures from -10 ºC to 50 ºC; concurrently with solar steam flow rates fluctuate from 0 to 100 percent of the HSSG steam mass flow at the design point, to estimate the steam turbine output. In each calculation, the steam turbine operates with flow rates and inlet temperatures, which are often significantly different from the design point conditions. A three dimensional curve fit of the ambient temperature, solar steam flow rate, and steam turbine output is developed and represented in Figure 4.28.

As shown in figure 4.26 and 2.28, the performance of the steam turbine is a weak function of the ambient temperature and a strong function of the thermal input from the collector field.

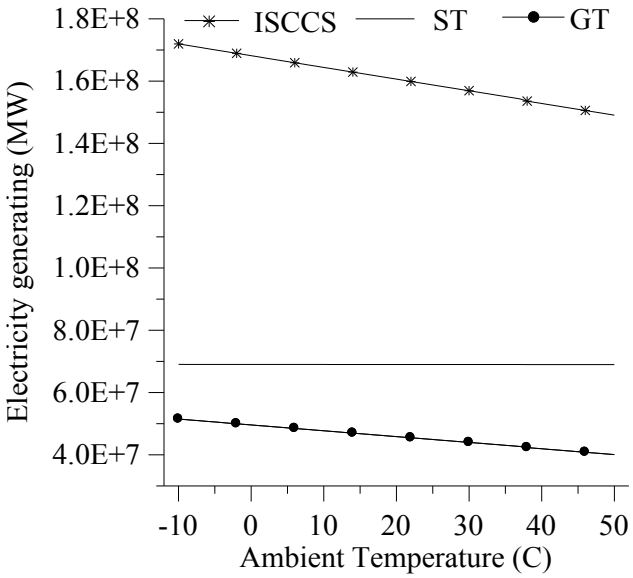

Figure 4.26: ST, GT, and ISCCS outputs as a function of ambient temperature.

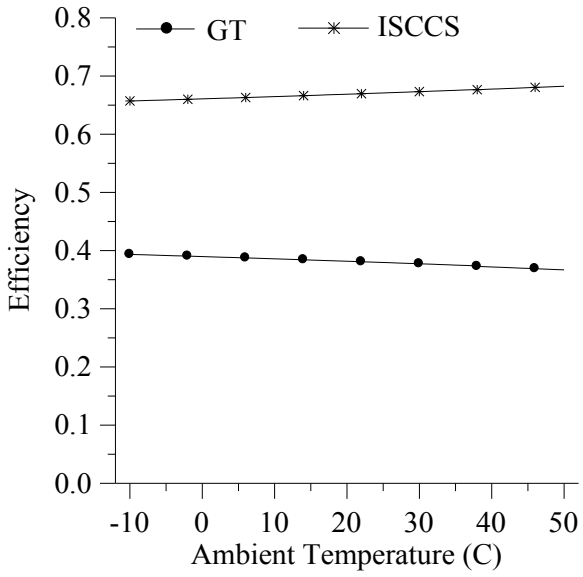

Figure 4.27: ST, GT, and ISCCS efficiency as a function of ambient temperature.

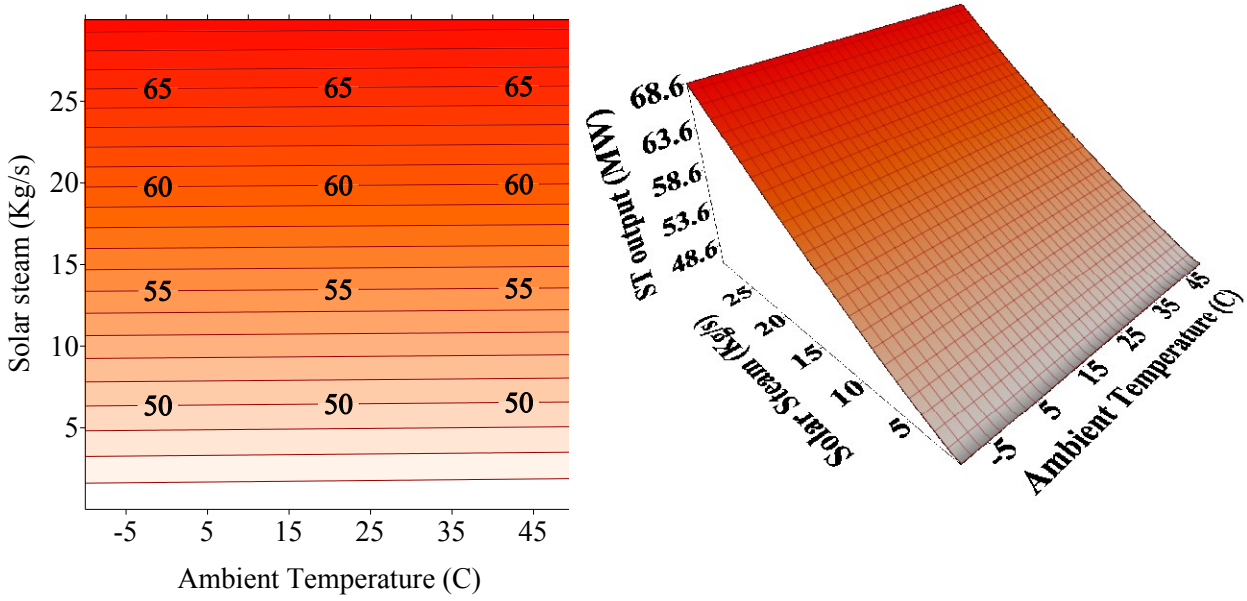

Figure 4.28: Steam turbine output as functions of ambient temperature and solar field output.

Consequently, the performance of the integrated plant was calculated in a manner similar to that for the conventional combined cycle plant. The principal exception was the performance of the steam turbine, which has a weak function of the ambient temperature and a strong function of the thermal input from the collector field.

RECOMMENDATIONS FOR FURTHER WORK

- Building a database of solar radiation and ambient conditions in Hassi R'mel location for a period of years is recommended to simulate the solar thermal power plants with real data.
- Design an optimum heat exchanger network by rationalizes the choice of the pressure levels and of the steam mass flows while respecting the off design operating conditions of the steam turbine (cone low) to achieve maximum steam turbine efficiency for the various operational modes.
- An economic assessment for the cost of exporting the electricity to the western countries in the Mediterranean from Algeria is also recommended.
- More comprehensive research about ISCCS based on real solar radiation data especially in winter when the fluctuation of solar radiation is very important at daytime.

CONCLUSION

A Computational software to simulate the performance of the first integrated solar combined cycle in Algeria has been developed under Hassi R'mel climatic conditions; whereby the different parts of the ISCCS were evaluated.

The gas turbine analytic solution is able to predict the gas turbine output with excellent accuracy. The gas turbine subprogram is used to calculate the rejected heat from the two gas turbines. This program is capable to be used in further work in many different applications. Such as, cogeneration power plants to predict the electricity generation and the drinking water desalination output.

The solar field subprogram predicts the solar field performance. In the present work, it is used to estimate the solar field input to the steam cycle simultaneously from sunrise to sunset through the estimation of the direct normal irradiation during the year. The program achieves 133 MW of solar thermal energy at the design point and about 100 MW from March through September, where this value is considered as a guarantee value by the designer company ABENGOA. An efficiency of 81% for the solar field is also achieved at the design point, which represents good results for the solar field efficiency. This program can be used in any further research which includes parabolic trough solar field. It can also be applied to estimate terrestrial solar radiation in all solar application such as solar tower, Fresnel technology, dish Stirling engine…

The integrated solar combined cycle system simulation results show that the model is capable to predict the output of the ISCCS under Hassi R'mel climatic conditions. The power plant responses sensibly to the solar radiation increase, where the electricity output increases accordingly to the solar radiation increase. The simulation results show that net solar electricity ratio can be very interesting and reach the limit of 15% at the design point. As a result, the ISCCS efficiency will be above the conventional combined power plant by 16.5%.

The advantage of this advanced power station results in electricity increase by 17% without burning any extra fossil fuel in the HRSG even in the gas turbines. The CC regime operation provides about 134MW at night. At daytime, solar energy can be converted to electricity with efficiency higher than at combined cycle mode because of the most efficient method for converting solar thermal energy to electric energy which is proposed in this research. Consequently, the ISCCS operation increases the plant capacity to 157 MW and the efficiency to 67% at the design point.

The sensitivity of the integrated plant at ambient temperature was calculated in a manner similar to that for the conventional combined cycle. The principal exception was the performance of the steam turbine, which has a weak function of the ambient temperature and a strong function of the thermal input from the solar field. Other advantages of ISCCS are increasing the steam turbine capacity of conventional combined cycle by 50% at the design point and better performances in warm days compared with the combined cycle power plants.

REFERENCES

[1] Allani Y., Favrat D., von Spakovsky M., 1996, CO2 mitigation through the use of hybrid solar combined cycles. Third Int. Confi. On Carbon Dioxide Removal Technologies (ICCDR-3), MIT, Cambridge, USA.

[2] Kane M., Favrat D., 1999, Approche de conception et d'optimisation de centrale solaire intégrée à cycle combiné inspirée de la méthode du pincement (partie I: paliers de récupération). Int. J. Therm., Vol 38, No 6: pp 501-511.

[3] Kane M., Favrat D., 1999, Approche de conception et d'optimisation de centrale solaire intégrée à cycle combiné inspirée de la méthode du pincement (partie II: réseaux d'échangeurs de chaleur). Int. J. Therm. Sci., Vol 38, No 6: pp 501-511.

[4] Favrat D., et al., 2000, Thermoeconomic Analysis of Advanced Solar-Fossil Combined Power Plants, Int. J. Applied Thermodynamics,Vol.3, (No.4), pp.191-198.

[5] Bruce Kelly, Ulf Herrmann, Mary Jane Hale, 2001, Optimization studies for Integrated Solar Combined Cycle Systems, Proceedings of Solar Forum 2001,Solar Energy: The Power to Choose ,April 21-25, 2001 Washington, DC.

[6] Jürgen Dersch et al., 2004, Trough integration into power plants—a study on the performance and economy of integrated solar combined cycle systems, Energy 29 947–959.

[7] R. Hosseini et al, 2005, Technical and economic assessment of the integrated solar combined cycle power plants in Iran, Renewable Energy 30 1541–1555.

[8] Gamal Elsaket, 2007, Simulating the integrated solar combined cycle for power plants application in Libya, Master of Science, School of Engineering, Cranfield University, Germany.

[9] Angela Patnode, 2006, Simulation and Performance Evaluation of Parabolic Trough Solar Power Plants, Master of Science, University of Wisconsin-Madison, USA.

[10] John A. Duffie, William A. Beckmann, 1991, Solar Engineering of Thermal Processes, second edition.

[11] Zekai Sen, 2008, Solar Energy Fundamentals and Modeling Techniques, Atmosphere, Environment, Climate Change and Renewable Energy, Istanbul Technical University, Faculty of Aeronautics and Astronautics, Dept. Meteorology, Turkey.

[12] El Hadi Malick Kane, 2002, Intégration et Optimisation Thermo économique et Environomique De Centrales Thermiques Solaires Hybrides, Thèse De Doctorat, Lausanne, Suisse.

[13] Alvarez and Eduardo Zarza, 2007, Concentrating Solar Thermal Power, Platform Solar de Almeria-CIEMAT, Taylor &Francis.

[14] R. Forristall, October 2003, Heat Transfer Analysis and Modeling of a Parabolic Trough Solar Receiver Implemented in Engineering Equation Solver, Technical Report, National Renewable Energy Laboratory, NREL, USA.

[15] Alex Lezuo, 2007, Combined-Cycle Power Plants, Siemens Power Generation, Taylor & Francis Group.

[16] Desmond E. Winterbone, Advanced Thermodynamics for Engineers, , Book, Thermodynamics and Fluid Mechanics Division, Department of Mechanical Engineering, UMIST.

[17] Meherwan P. Boyce, 1997, Gas Turbine Engineering Handbook, Second Edition, Institute of Diesel and Gas Turbine Engineers, U.K.

[18] Philip P. Walsh, 2004, Head of Performance and Engine Systems, Rolls-Royce plc, Paul Fletcher, Manager, Prelim Design, Energy Business, Rolls-Royce plc, Gas Turbine Performance, Second Edition, Blackwell Science Ltd.

[19] Steam turbines for solar thermal power plants, 2008, Industrial steam turbines, Siemens AG, Energy Sector, Taylor &Francis.

[20] Abengeoa solar, Solar Power for a Sustainable World, Abengoa: a leader in sustainable development, April 24th, 2009.

[21] B. Kelly, 2005, National Renewable Energy Laboratory, Nexant Parabolic Trough Solar Power Plant Systems Analysis , Nexant, Inc. San Francisco, California

[22] E. Prabhu, 2005, Solar Trough Organic Rankine Electricity System (STORES), National Renewable Energy Laboratory, Reflective Energies Mission Viejo, California

[23] H. Price, 2003, National Renewable Energy Laboratory, A Parabolic through solar power plant simulation model, International Solar Energy Conference Hawaii Island.

[24] Hank Price and Vahab Hassani, 2002, Modular Trough Power Plant Cycle and Systems Analysis, Barber-Nichols, Exergy, Inc.

[25] Ahmed Khadim, 2008, l'énergie solaire, utilisation thermique et photovoltaïque, Institut solaire de l'université des sciences appliquées, Germany.

[26] Quoilin Sylvain, 2007, Centrales solaires à concentration, Université de Liège, Faculté des sciences appliquées.

[27] H.Derbal, 2005, Etude d'un système de production d'hydrogène par voie solaire, application à l'électrolyse de la vapeur d'eau à haute température, mémoire de magister, Universite des sciences et des technologies Houari Boumediene (USTHB), Algérie.

[28] Concentrated solar thermal power- now, 2005, European solar thermal power industry association ESTIA, solar space.

[29] George Barakos, 2006, Design, Simulation and performance of reflecting parabolic solar collector, Department of mechanical engineering, Technical educational institute of Para.

[30] Energies Renouvelables: Projet de Puissance, Rapport industrielle, Filière Solaire Thermique-Gaz Naturel. NEAL, Algérie.

[31] D. Yogi Goswami, Frank Kreith, Jan F. Kreider, Principles of solar engineering, 2nd Edition: Taylor &Francis.

[32] Eau chaud solaire, avril 2002, Manuel pour la conception, le dimensionnement et la réalisation des installations collectives, Agence de l'Environnement et de la Maîtrise de l'Energie.

[33] Eléments de résumé pour l'étude du potentiel vendéen et des applications possibles de l'énergie solaire thermique et photovoltaïque - Alliance Soleil SARL – Février 2007.

[34] Alain Ferriere et Gilles Flamant, Captation, transformation et conversion de l'énergie solaire par les technologies à concentration, IMP-CNRS, Centre du Four Solaire, BP5, 66125 Font-Romeu.

[35] Copyrighted Materials, 2003, Solar Irradiance, John Wiley- sons Retrieved from WWW.Knovel.com